J. Phys. G: Nucl. Part. Phys. **36** (2009) 113101 (43pp) doi:10.1088/0954-3899/36/11/113101

TOPICAL REVIEW

Multinucleon transfer processes in heavy-ion reactions

L Corradi[1], G Pollarolo[2] and S Szilner[3]

[1] Istituto Nazionale di Fisica Nucleare, Laboratori Nazionali di Legnaro, I-35020 Legnaro, Italy
[2] Dipartimento di Fisica Teorica, Università di Torino and Istituto Nazionale di Fisica Nucleare, I-10125 Torino, Italy
[3] Ruđer Bošković Institute, HR-10 001 Zagreb, Croatia

E-mail: lorenzo.corradi@lnl.infn.it, nanni@to.infn.it and szilner@irb.hr

Received 22 July 2009
Published 25 September 2009
Online at stacks.iop.org/JPhysG/36/113101

Abstract
The main advances in the field of multinucleon transfer reactions at energies close to the Coulomb barrier are reviewed. After a short presentation of the experimental techniques and some gleams from the theory the new data are presented. The possibilities offered by the coupling of large γ-array detectors with tracking spectrometers are discussed.

(Some figures in this article are in colour only in the electronic version)

1. Introduction

Transfer reactions play an essential role in the study of the structure of nuclei; with light ions, they provided important data for the construction of the shell model and to establish the properties of particle–particle correlations in the nuclear medium [1–3]. With heavy ions, transfer reactions played a very important role for the definition of the reaction mechanism [4] that describes the evolution of the reaction from the quasi-elastic regime to the more complex deep-inelastic and fusion [5]. At least for energies close to the Coulomb barrier, transfer constitutes the largest part of the total reaction cross section [6] thus providing the main source for the loss of flux from the elastic channel and the main mechanism for the energy dissipation from the relative motion to the intrinsic excitation. With heavy-ions multiple transfer of nucleons becomes available in the reaction giving the possibility to study the relative role of single particle and pair transfer modes [7]. Excited states in final nuclei are populated with significant strength, providing information on the contribution of surface vibrations (bosons), single particles (fermions) and their coupling.

In the last decade, the renewed interest in transfer reactions has been mainly due to the realization that multinucleon transfer reactions could be used to populate nuclei moderately rich in neutrons [8, 9]. It is in this region of the nuclear chart that the most challenging aspects in the behavior of the nuclear structure have been foreseen, for instance, the evolution

of shell gaps or the role of the tensor component [10] of the nucleon–nucleon interaction. This renewed interest benefited from the construction of the new generation large solid angle spectrometers based on trajectory reconstruction, with which one could gain more than an order of magnitude in overall efficiency still keeping a good identification of reaction products [11, 12]. The coupling of these spectrometers with large γ arrays [13, 14] allowed the identification of γ rays coming from the decay of weak transfer channels associated with the population of nuclei moderately far from stability.

Significant advances in calculations have been achieved. Making use of the semi-classical approximation [4, 15] it has been possible to extend in the reaction model the concept of elementary modes of excitation [16, 17] that have been very successful in the interpretation of nuclear spectra. The concept of elementary modes of excitation allowed to develop models [18] that are able to treat quasi-elastic and deep-inelastic processes on the same footing and to quantitatively study reactions that involve the transfer of many nucleons. The models are in fact able to predict how the total reaction cross section is shared amongst the different channels. The understanding of these processes is important, in particular, in view of research to be done with radioactive beams [8, 19]. This is also important for the understanding of sub-barrier fusion cross sections. Recent work on the subject can be found in the conferences [20, 21] and references therein.

In this work, we review the main advances in the field done in the last few years. After a presentation of the more recent experimental techniques we will discuss in some details the main characteristics of multinucleon transfer reaction evidencing the validity of the elementary modes of excitation and introducing the semi-classical approximation that will be our guide throughout the review. We will discuss differential and total cross sections and total kinetic energy loss distributions and the connection between multinucleon transfer reactions and other competing reaction channels. A discussion on some recent results of γ-particle coincidence measurements will also be presented.

2. Detection techniques for heavy-ion transfer products

Different techniques have been employed to identify nuclei produced in transfer reactions. Most of these techniques make use of magnetic spectrographs or spectrometers for a complete identification of nuclear charge, mass and energy of final reaction products and to provide at the same time absolute differential and total cross sections.

The development of magnetic spectrographs emerged in the past from the need to distinguish excited states populated in light ion transfer reactions. This was achieved by combining magnetic elements of different complexity to focus momenta at definite positions on the focal plane. With these instruments, that required corrections for ion optical aberrations, an energy resolution of the order of a few tenths keV could be achieved. Q3D or split pole devices have been extensively used for studies of one and two particle transfer reactions (see [6] and references therein), and Q3D with an improved energy resolution ($\leqslant$10 keV) are still employed for detailed spectroscopic studies [22].

With heavier ions more demanding conditions are required in order to keep a good resolution and to have at the same time a sufficient detection efficiency, given the large energy dynamic range of transfer products. Solutions have been adopted to deal with the increase of energy and angular straggling with ions of higher nuclear charge with emphasis on the complexity of magnetic elements and/or on the detector systems. Some characteristics of Q3D magnetic configurations have been kept for instance in the ENMA spectrograph [23], which was especially designed for studies of elastic, inelastic and transfer reactions with ions in the mass range $50 \leqslant A \leqslant 90$. Split poles, with a simpler magnetic configuration, have been

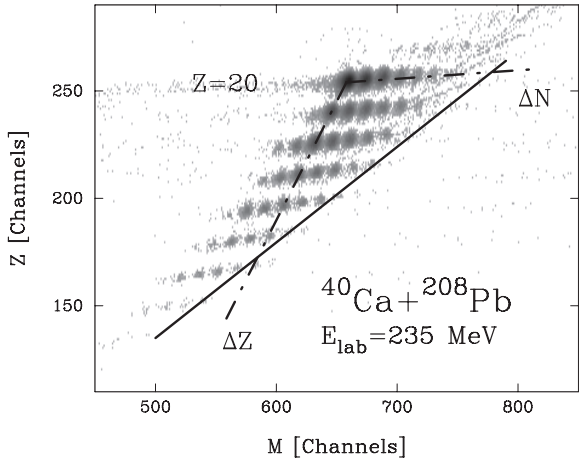

Figure 1. Mass–charge distribution of transfer products in the ^{40}Ca+^{208}Pb reaction at E_{lab} = 235 MeV obtained at the grazing angle, $\theta_{lab} = 84^{\circ}$. The dash-dotted lines correspond to the pure proton stripping (ΔZ) and to the pure neutron pick-up (ΔN) channels, crossing at $Z = 20$ and $A = 40$. The full line shows the charge equilibration, namely, the N/Z ratio of the compound nucleus (from [32]).

extensively used in the same mass region to measure yield distributions and cross sections in the quasi-elastic regime [6, 24]. In all these devices, in order to obtain the cross sections for the different exit channels, the distribution of atomic charge states has to be carefully taken into account. To (partially) handle this problem, time-of-flight (ToF) spectrometers have been designed with magnetic quadrupole elements which focus ions of different atomic charge states to a relatively small focal plane [25–27]. In split poles as well as in ToF spectrometers a good A and Z resolution for medium mass ions could be preserved, although with energy resolution of the order of a few MeV, i.e. lower compared with the spectrographs mentioned above.

Recoil mass spectrometers [28] employ a combination of magnetic and electric elements to provide directly mass identification, and have been designed to separate ions with different electric rigidities (compound nuclei and beam-like particles). Even if not originally constructed for quasi-elastic reactions, these devices have been used in some cases for studies at sub-barrier energies detecting the (higher mass) target recoils at angles close to $\theta_{lab} = 0^{\circ}$ (i.e. $\theta_{cm} = 180^{\circ}$) where transfer cross sections peak [29]. However, the low kinetic energy of the recoils prevents to get a sufficient Z and energy resolutions.

Inverse kinematics has been often employed to achieve a sufficient separation of the outgoing transfer products. Detecting the lighter (than projectile) target-like recoils at forward angles, one has a high efficiency (kinematic focusing) and a good resolution (high kinetic energy) [30, 31]. Of course, this technique requires a very good rejection of the primary beam and needs the use of very pure targets when dealing with low transfer cross sections.

The quality of data presently achieved is demonstrated in figure 1 where it is shown, as a representative example, the mass and charge distribution of transfer products in the ^{40}Ca+^{208}Pb system [32] identified with a time-of-flight spectrometer. Here the mass is obtained by using the time of flight between the entrance and focal plane detectors of the spectrometer, where total energy and Z are extracted from a multiparametric ionization chamber [33]. A clear identification of the transfer products is obtained up to the pick-up of approximately six

neutrons and the stripping of approximately six protons. The bombarding energy is close to the Coulomb barrier and the yield, measured at the grazing angle, reflects some of the main characteristics of quasi-elastic processes. These may be appreciated by plotting on the same figure three lines, the two dash-dotted lines correspond to pure neutron pick-up and pure proton stripping channels, while the full line represents the charge equilibration, namely the location of the N/Z ratio of the compound nucleus. The fact that most nuclei are located on the left side of the charge equilibration line indicates the dominance of a direct mechanism in the population of different fragments. Note also that for the massive proton transfer channels the isotopic distributions drift toward lower masses, a clear indication that these distributions are affected by evaporation processes (these aspects will be extensively discussed in the following sections).

In dealing with heavier and heavier ions, to preserve nuclear charge and mass separation (via ToF and energy), apart from reaching sufficient kinetic energy, position information becomes crucial. The GSI magnetic spectrometer, designed for very heavy ions [34], combines a multiparametric focal plane detector with a sequence of magnetic elements, where the dipole provides the momentum over atomic charge (p/q) dispersion. The combination of multipole magnetic elements and the position information at the entrance and focal plane of the spectrometer allows us to handle and correct for optical aberrations up to some order. With this instrument, the yield distribution and cross sections of multinucleon transfer channels have been studied in various angular ranges using beams in the mass range $A \simeq 90$–208 on heavy targets [35, 36]. Here, also, inverse kinematics has been successfully employed.

2.1. Large acceptance magnetic spectrometers

The discussed devices have solid angles in the range 3–10 msr. Beyond these values, it becomes unfeasible to use complex magnetic elements to correct for the ion optical aberrations. At the same time one has to consider the kinematics of grazing collisions, where a wealth of nuclei are produced in a wide energy and angular range and with cross sections spanning several orders of magnitude, thus putting extremely demanding requests on the detection system. The presently adopted solution is to simplify the magnetic element configuration and to apply the concept of trajectory reconstruction. This can be done by using a detector system which, besides nuclear charge, energy and timing, provides the necessary position information along the ion path. To reconstruct the ion path through the spectrometer specially developed algorithms are then adopted, whose complexity depend on how precise is the experimental knowledge of ion transport.

The idea to use a 'simple' magnetic configuration and an event-by-event reconstruction of the ion trajectory inside magnetic elements to identify the transfer reaction products, has been successfully employed in the very large solid angle ($\sim$100 msr) spectrometers PRISMA [11], VAMOS [12] and MAGNEX [37]. In PRISMA, the reconstruction of the ion trajectory is obtained from the measurement of an entrance [38] and focal plane positions [39], together with the time of flight. In between these two detector systems only two magnetic elements are located, a quadrupole followed by a dipole. The large longitudinal dimension of the dipole compared with the transversal one ensures a weak effect of the fringing fields and the planarity of the trajectory. The tracking procedure provides the curvature of ion path inside the dispersive (dipole) element for a unique determination of the trajectory and leads to a quantity proportional to p/q. PRISMA has a fixed momentum dispersion while VAMOS can be used in a variable dispersive mode at the focal plane [40] depending on the chosen deflection angle of the dipole, and it is equipped with a Wien filter to help selecting ions of different rigidities. In VAMOS, one measures the position and angle of ions after the magnetic elements and the reconstruction

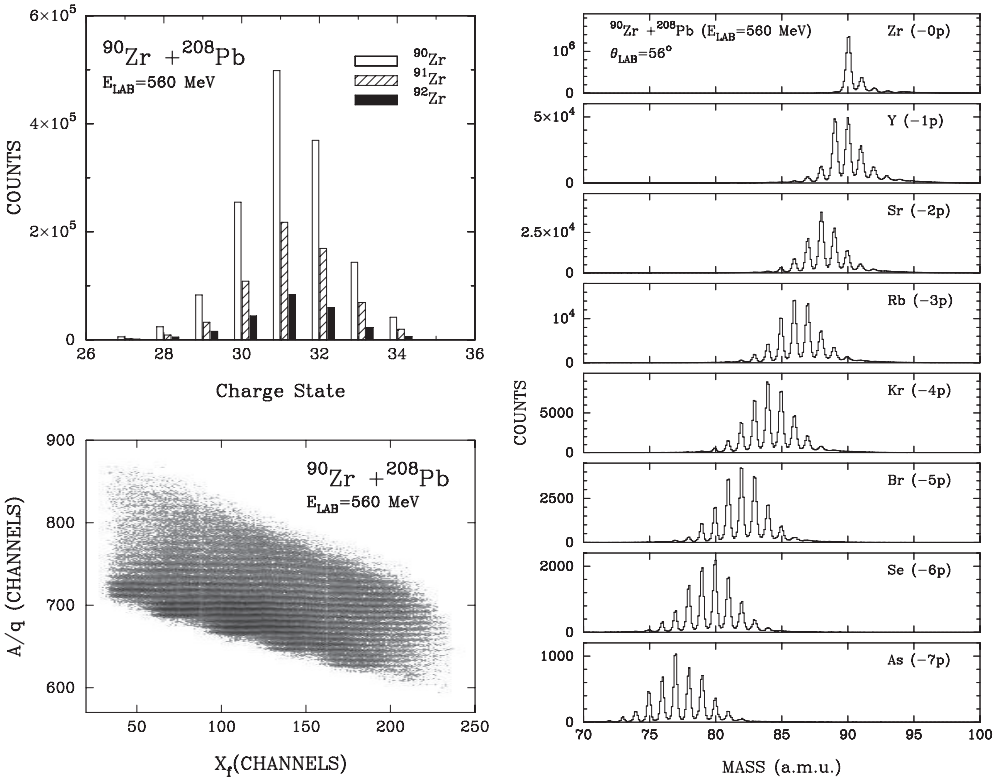

Figure 2. Left top panel: atomic charge state distribution for ^{90,91,92}Zr ions selected with PRISMA in the reaction ^{90}Zr+^{208}Pb at $E_{\rm lab} = 560$ MeV. Left bottom panel: mass over atomic charge state A/q versus horizontal focal plane position $X_{\rm f}$. Right panel: mass distributions of transfer products for different Z (adapted from [41]).

is made through an inverse transformation of coordinates from the focal plane to the target, via ray tracing procedure. This solution avoids using a position sensitive detector close to the target but needs a more complex software procedure.

In the left bottom panel of figure 2, we show as representative example a matrix of the mass over atomic charge state (A/q) versus the longitudinal position on the focal plane for Zr-like products in the reaction ^{90}Zr+^{208}Pb [41], obtained with PRISMA. One sees the achieved resolution and the characteristic repetitive pattern of the different A/q.

To derive the mass from this ratio, one must get the atomic charge state. The left top panel and right panels of figure 2 show the extracted atomic charge state distribution for the zirconium isotopes and the mass distributions of transfer products, respectively. As said before, in grazing collisions nuclei are produced in a broad angular and kinetic energy range, with nuclear charge and mass differing by several units from the entrance channel. The ion transmission through these large solid angle spectrometers depends in a complex way on the in-plane and out-of-plane entrance positions and momenta and a careful procedure have to be employed to get absolute cross sections. A determination of the transmission is generally achieved via a simulation of ion trajectories, where the kinematics of the reaction and the geometry of the magnetic elements and detectors is taken into account.

2.2. *Magnetic spectrometers with γ-detector arrays*

With these new generation spectrometers, mass and nuclear charge identification has been successfully demonstrated for ions up to $A \simeq 100$–130, but energy resolution is presently limited to few hundreds of keV. Though excited state discrimination can be performed in suitable nuclei where levels are sufficiently separated, spectrometers cannot compete yet with the highest energy resolution achieved by the use of high purity germanium γ detectors. Large γ arrays have been proved to be very powerful tools for nuclear spectroscopy studies of nuclei produced in transfer reactions, especially for very heavy nuclei [7, 42, 43]. Double and triple γ coincidences could be performed in experiments using thick targets, where all products are stopped. A different and complementary approach is to use, with thin targets, a coincidence between γ and particle detectors, where a Doppler correction has to be applied for the γ rays emitted by the moving ions. This coincidence method, though lowering the overall efficiency, allows us to define the impact parameter of the transfer reaction (angular distribution) and helps to reduce undesired events coming from other reaction channels. Position sensitive gas detectors of large area have been often employed, and if used in kinematic coincidence (both partners in the binary reaction are detected) a low resolution determination of mass and Q-value can be done [44]. By gating on different ranges of these quantities, selected excitation energy regions of nuclei can be studied looking at their γ decay. Gas detector systems covering a large fraction of the angular range of transfer products in different heavy-ion reactions have been used coupled to large γ arrays [45–47]. With the further possibility to measure γ multiplicity the population strength of transfer products can be investigated in different regions of (deduced) spin versus excitation energy. We here remark that to derive absolute cross sections of transfer products from γ-ray intensities only, detailed knowledge of the decay levels, branching and population pattern is mandatory. This is not a straightforward procedure, as for instance in the case of odd nuclei where the population strength can be significantly fragmented or for heavy nuclei with significant EC decay fraction.

The method of particle-γ coincidences has been further employed by coupling large γ arrays to the new generation large solid angle spectrometers discussed above, which provide at the same time a full identification of the reaction products and their absolute yield. The Doppler correction in this case is done from the knowledge of the reconstructed velocity vector. As an example of this procedure we plot in figure 3 (top) the total kinetic energy loss (TKEL) measured in the ionization chamber of the PRISMA spectrometer for the +2n channel (^{92}Zr) produced of the ^{90}Zr+^{208}Pb reaction. Its associated γ-ray spectra are shown in the bottom part of figure 3, obtained without (top panel) and with (middle and bottom panels) different conditions on the TKEL. This demonstrates how, by gating on selected TKEL regions, one can enhance/suppress transitions between states with different excitation energy and angular momenta. By gating on the low TKEL region (A) the two lowest yrast transitions dominate the spectrum. By gating instead on the TKEL region around 20 MeV (B) the spectrum displays transitions coming from the decay of high spin states (we remark that the excitation energy of both light and heavy fragments is embedded into the TKEL distribution).

A very important use of the γ-particle coincidence technique which employs the new generation spectrometers in terms of resolution and efficiency is for studies of nuclei moderately far from stability whose structure is poorly or not known at all. At variance with reactions (like fusion evaporation) where the γ cascade proceeds from high-level density regions and ends-up in yrast states, grazing reactions favor a certain degree of direct population of final states, also of non-yrast character. As shown before, the further possibility to experimentally choose regions of Q-value distribution and impact parameter of the reaction

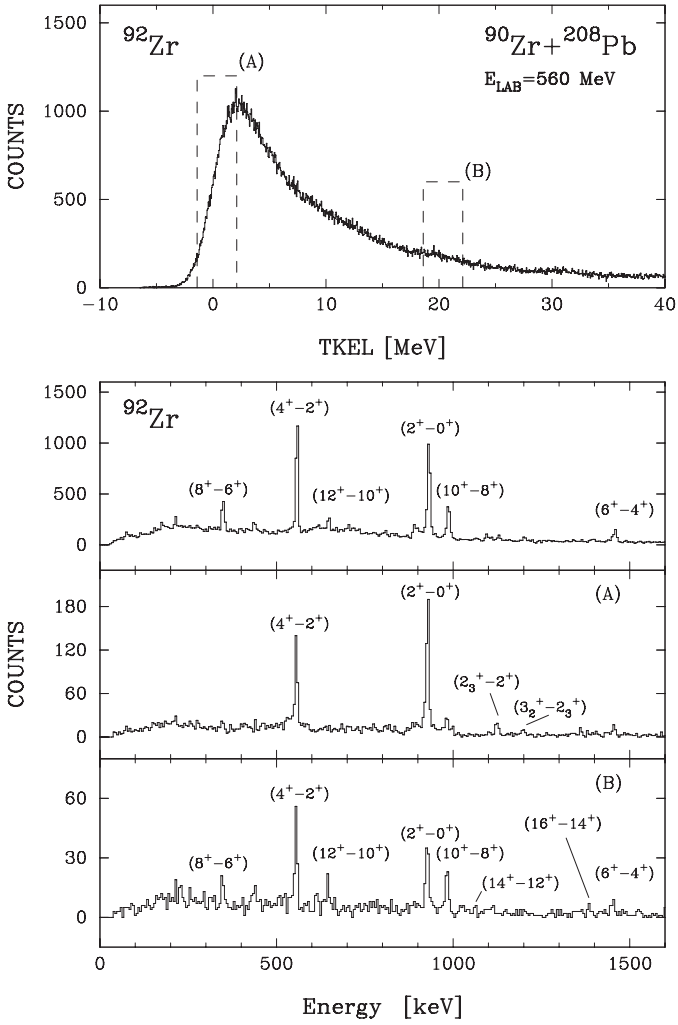

Figure 3. Top: TKEL distribution for ^{92}Zr produced in the ^{90}Zr+^{208}Pb reaction. Bottom: associated γ-ray spectra for ^{92}Zr without conditions on TKEL (up) and conditioned (middle and down) with different regions of TKEL distributions, marked as (A) and (B) in the TKEL spectrum and with gates $\simeq$3 MeV wide. Typical γ ray energy resolution obtained after Doppler correction are 0.6–0.9% FWHM over the whole velocity distribution (from [41]).

(angle) facilitates the study of states associated with specific excitation energy. Very often, the detection of few γ transitions belonging to nuclei identified in mass and nuclear charge with spectrometers allows a consistent analysis of double and triple γ coincidence data collected independently with γ arrays only and obtained by exploiting the same kind of reaction mechanism [9].

3. Gleams from the theory of transfer reactions

In the first part of this section we recall, in a simplified form, the coupled-channel formalism that is at the base for any description of direct reaction processes. The total wavefunction $|\Psi^+\rangle$

is expanded in terms of channel wavefunctions $|\psi_\beta\rangle = |\psi_b\psi_B\rangle$

$$|\Psi^+\rangle = \sum_\beta \frac{\chi_\beta(r_\beta)}{r_\beta}|\psi_\beta\rangle, \tag{1}$$

where $|\psi_b\rangle$ and $|\psi_B\rangle$ are the two wavefunctions describing the intrinsic states of the two nuclei belonging to the $\beta \equiv (b, B)$ mass partition and χ_β is the corresponding wavefunction for the radial motion. By requiring that (1) is a solution of the time-independent Schrödinger equation

$$[H_0 + V]|\Psi^+\rangle = E|\Psi^+\rangle \tag{2}$$

one obtains the following system of coupled equations:

$$\frac{\mathrm{d}^2\chi_\beta(r_\beta)}{\mathrm{d}r_\beta^2} + \frac{2\mu_\beta}{\hbar^2}\left[E_\beta - V_\beta^{\mathrm{eff}}(r_\beta)\right]\chi_\beta(r_\beta) = \frac{2\mu_\beta}{\hbar^2}\sum_{\gamma\neq\beta} V_{\beta\gamma}^{\mathrm{cpl}}(r_\beta, r_\gamma)\chi_\gamma(r_\gamma) \tag{3}$$

where

$$V_\beta^{\mathrm{eff}}(r_\beta) = \frac{\hbar^2}{2\mu_\beta}\frac{\ell_\beta(\ell_\beta+1)}{r_\beta^2} + \langle\psi_\beta|V|\psi_\beta\rangle \tag{4}$$

is the effective potential and

$$V_{\beta\gamma}^{\mathrm{cpl}}(r_\beta, r_\gamma) = \langle\psi_\beta|V|\psi_\gamma\rangle \quad \beta \neq \gamma \tag{5}$$

are the coupling matrix elements. In the above expressions, $H_0 = H_b + H_B + T_{bB}$ is the Hamiltonian for the intrinsic states of the two ions (H_b and H_B) and for the relative motion (T_{bB}), V the coupling interaction, μ_β the reduced mass of channel β and E_β is the corresponding channel energy. The radial wavefunction χ_β, solution of the system of coupled equations, is obtained by requiring that $\chi_\beta = 0$ at the origin and matches the asymptotic form of an incident wave of unity norm for the entrance channel and an outgoing radial wave in all other channels. From the amplitudes of the outgoing waves one extracts the corresponding reaction cross sections.

In writing down the system of coupled equations, where the angular momentum coupling has been neglected to simplify the notation, some approximations have been done. Since the total number of nucleons can be partitioned in several ways, the channel wavefunctions $|\psi_\beta\rangle$ form an over-complete base of non-orthogonal vectors. The problem of over-completeness is normally overcome by including in the summation only bound or quasi-bound states belonging to the different mass partitions and by imposing a boundary condition at a suitable point (incoming wave boundary condition), or by including an imaginary potential to account for the depopulation of the entrance channel due to channels not explicitly included in the system of coupled equations. The (mostly technical) treatment of the non-orthogonality, which is relevant when transfer channels are included, complicates considerably the formalism, in equation (3) all terms deriving from the non-orthogonality are neglected. In the regime of direct reactions, these contributions are usually small due to the weak overlap of the two ion densities.

An alternative treatment to the quantal system of coupled equation (3) has been obtained [4] by generalizing the well-known semiclassical theory of Coulomb excitation [48] to include the effect of the nuclear interaction. We recall that the semiclassical approximation, where the relative motion is treated classically, is valid also at energies above the Coulomb barrier since the wave length associated with the relative motion is much smaller than the interaction region (sum of the two nuclear radii). The total wavefunction of the system is in this case written in the form

$$\Psi(t) = \sum_\beta c_\beta(t)\psi_\beta\, \mathrm{e}^{-\mathrm{i}(E_\beta t + \delta_\beta(t))/\hbar}, \tag{6}$$

where the time-dependent coefficient $c_\beta(t)$ defines the amplitude to be in channel β and ψ_β is the channel wavefunction introduced above. The (time-dependent) phase δ_β, included to take into account that the relative motion of the two ions does not follow a straight line, is defined as

$$\delta_\beta(t) = \int^t \mathcal{L}_\beta(t)\,\mathrm{d}t \tag{7}$$

with $\mathcal{L}_\beta$ being the Lagrangian of relative motion. Inserting the expansion (6) in the time-dependent Schrödinger equation:

$$\frac{\partial\Psi(t)}{\partial t} = [H_0 + V]\Psi(t), \tag{8}$$

one obtains the following system of semi-classical coupled equations:

$$\frac{\mathrm{d}}{\mathrm{d}t}c_\beta(t) = \frac{\mathrm{i}}{\hbar}\sum_\gamma \langle\omega_\beta|(V_\gamma - U_\gamma)|\psi_\gamma\rangle c_\gamma(t)\,\mathrm{e}^{-\mathrm{i}[(E_\gamma - E_\beta)t - (\delta_\gamma(t) - \delta_\beta(t))]/\hbar}. \tag{9}$$

This system has to be solved with the condition that at $t = -\infty$ it is in its entrance channel α, i.e. $c_\beta(t = -\infty) = \delta_{\alpha\beta}$.

The vectors $|\omega_\gamma\rangle$ constitute a dual base that is introduced to overcome the problem of the non-orthogonality of the vectors $|\psi_\gamma\rangle$. This dual base is easily constructed from the overlap matrix $O_{\beta\gamma} = \langle\psi_\gamma|\psi_\beta\rangle$. The time dependence of the matrix elements in equation (9) is obtained by solving the Newtonian equations for the relative motion that develops in a nuclear (U_γ) plus Coulomb field.

3.1. Coupling matrix elements

The most important components of equations (3) and (9) are the matrix elements, that weight the relative importance of the different channels. These may be divided into two categories, one responsible for the inelastic excitation and the other for the exchange of nucleons between the two partners. For the inelastic excitation one usually employs the macroscopic approximation that allows us to write the radial part of the form factor as the r-derivative of the potential

$$f_\lambda^{\mathrm{inel}}(r) = \beta_\lambda \frac{\partial U(r)}{\partial r}, \tag{10}$$

where β_λ is the deformation parameter that bears information on the collectivity of the state and $U(r)$ is the average potential of entrance and exit channels.

In the case of particle transfer [49, 50] the matrix elements are non-local functions of the center-of-mass coordinates of the two channels. This dependence, normally referred as recoil effect, may be translated into a dependence on the momentum transfer $\vec{\kappa}$,

$$\langle\omega_\beta|(V_\gamma - U_\gamma)|\psi_\gamma\rangle = f_{\beta\gamma}(\vec{\kappa}, \vec{r}), \tag{11}$$

where $\vec{r}$ is

$$\vec{r} = \tfrac{1}{2}(\vec{r}_\beta + \vec{r}_\gamma) \tag{12}$$

r_β and r_γ being the center-of mass distances in channels β and γ, respectively, as shown in figure 4. The most important component of the recoil, namely the dependence of the form factor on the transferred momentum $\vec{\kappa}$, is its transversal component that may be taken into account through a phase factor

$$f_{\beta\gamma}(\vec{\kappa}, \vec{r}) \sim \mathrm{e}^{\mathrm{i}\sigma_{\beta\gamma}t} f_{\beta\gamma}(0, \vec{r}) \tag{13}$$

with

$$\sigma_{\beta\gamma} \sim \frac{1}{\hbar}\frac{m_d}{m_b + m_B}\dot{r}(t)(R_B m_c - R_b m_C), \tag{14}$$

where m_d is the mass of the transferred particle and $\dot{r}(t)$ is the radial velocity.

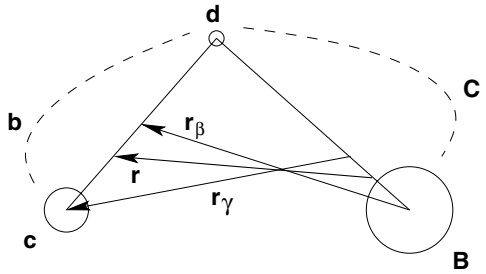

Figure 4. Coordinate system used in the definition of the transfer form factor. c and B are the cores in projectile-like and target-like and d is the transferred particle.

The radial dependence of the transfer form factor may be calculated explicitly by a folding integral that involves the residual interaction and the two wavefunctions describing the motion of the transferred particle d around the cores of projectile-like and target-like. By using the simple parametrization of [51] the particle transfer form factor can be written as

$$f_{\beta\gamma}(0, r) \sim k_\lambda(\kappa_{a_1'} r), \tag{15}$$

where k_λ is related to the Hankel functions that describe the asymptotic behavior of the bound-state wavefunction, λ being the angular momentum transfer. At large distances we can write

$$f_{\beta\gamma}(0, r) \propto \frac{1}{\kappa_{a_1'} r} \mathrm{e}^{-\kappa_{a_1'} r}. \tag{16}$$

The asymptotic behavior of the form factor is governed by the coefficient $\kappa_{a_1'}$ that contains the binding energy of the single particle state a_1' entering in the transition. For single particle states close to the Fermi energy the decay length of the one-particle transfer form factor is of the order of 1.2 fm, thus at large distances the transfer form factor prevails over the nuclear component of the inelastic form factor. In figure 5, the radial dependence of the one-particle transfer form factors is shown for different systems in comparison with the simple parametrization of [51].

3.2. Q-value dependence of the cross sections

To estimate the magnitude of a given transfer process it is not necessary to solve explicitly the full system of coupled equations but it suffices to write down its first-order Born approximation. For a given impact parameter (incoming partial wave ℓ) the probability for the transition from the entrance channel α to the channel β may be written in the form

$$P_{\beta\alpha}(\ell) = \left| \frac{\mathrm{i}}{\hbar} \int_{-\infty}^{+\infty} \mathrm{d}t \, \mathrm{e}^{\mathrm{i}\sigma_{\beta\alpha} t} f_{\beta\alpha}(0, \vec{r}) \, \mathrm{e}^{\mathrm{i}[(E_\beta - E_\alpha) + (\delta_\beta - \delta_\alpha)]t/\hbar} \right|^2, \tag{17}$$

where the time integral has to be performed along the classical trajectory for the given partial wave ℓ. In direct processes the two nuclei barely overlap, so that only the tail of the form factor is relevant. By approximating the true trajectory with a parabolic parametrization around the turning point the above transition probability may be written in the form

$$P_{\beta\alpha} = \sqrt{\frac{1}{16\pi\hbar^2 |\ddot{r}_0| \kappa_{a_1'}}} |f_{\beta\alpha}(0, r_0)|^2 g(Q_{\beta\alpha}), \tag{18}$$

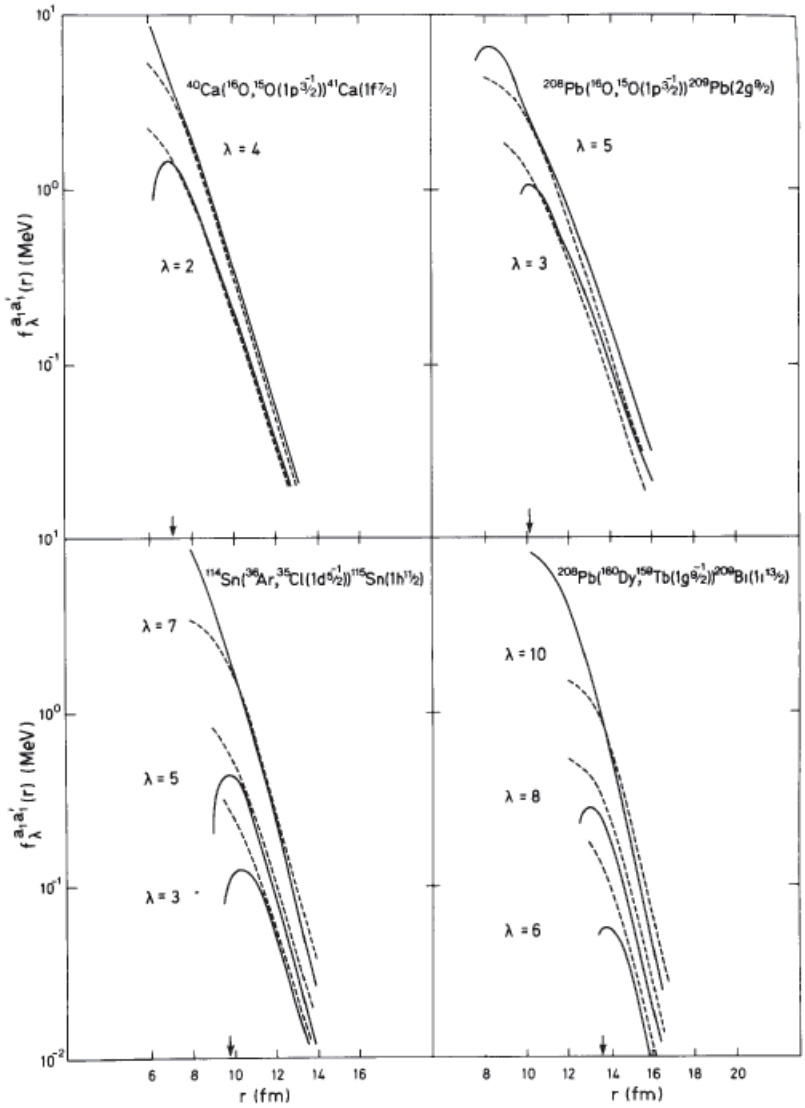

Figure 5. Comparison between the simple parametrization of [51] (dash line) with the exact calculations (full line) for several examples of single particle transitions among indicated projectile and target combinations (adapted from [51]).

where $\ddot{r}_0$ is the radial acceleration at the distance of closest approach r_0 for the grazing partial wave. The adiabatic cut-off function $g(Q)$ is defined as

$$g(Q) = \exp\left(-\frac{(Q - Q_{\text{opt}})^2}{\hbar^2 \ddot{r}_0 \kappa_{a'_1}}\right), \tag{19}$$

where the optimum Q-value is

$$Q_{\text{opt}} = \left(\frac{Z_d}{Z_A} - \frac{Z_d}{Z_b}\right) E_B + \left(\frac{m_d}{m_b} - \frac{m_d}{m_A}\right)(E - E_B) + \frac{m_d \ddot{r}_0}{m_a + m_A}(R_A m_b - R_a M_B), \tag{20}$$

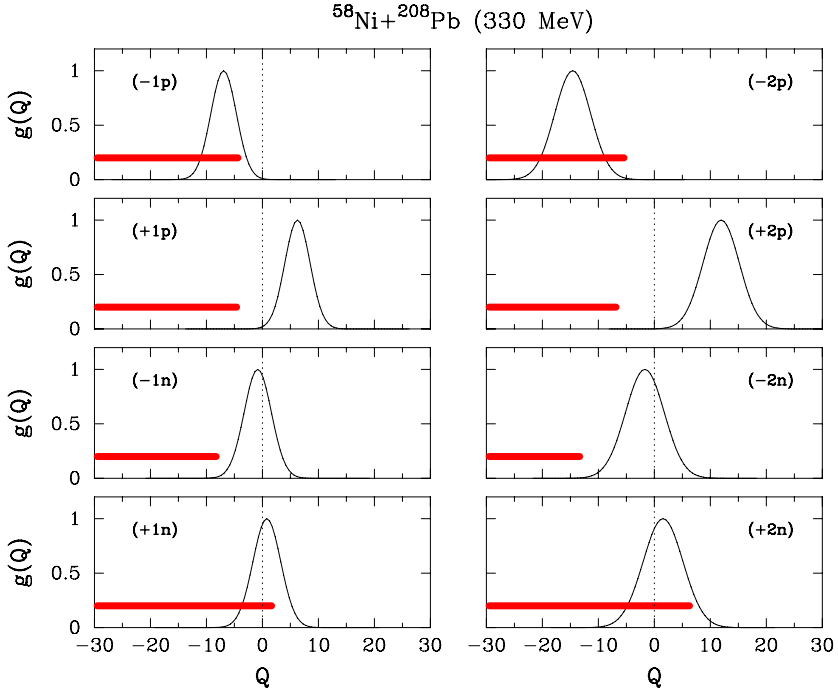

Figure 6. Adiabatic cut-off functions for one- and two-neutron and proton transfer channels for the reaction ^{58}Ni+^{208}Pb at the indicated energy (Q-value in MeV). The horizontal lines represent the location of all possible transitions.

E_B is the Coulomb barrier and m_d and Z_d are the mass and charge of the transferred particle. The adiabatic cut-off function $g(Q)$ defines the actual value of the transition probability, the maximum being at the optimum Q-value. This derives from the requirement that the trajectory of entrance and exit channels matches smoothly close to the turning point where the contribution of the form factor peaks. We note that the bombarding energy dependence of the cut-off function is contained in the $\ddot{r}_0$ term that defines its width (inversely proportional to the collision time).

A rough estimation of the total cross section for a particular transfer channel can be obtained by simply performing a Q-value integration of equation (18). In figure 6, for the ^{58}Ni+^{208}Pb reaction we show the adiabatic cut-off function $g(Q)$ for all one- and two-particle transfer channels. In the same figure with horizontal lines we represent, for all channels, the location of all possible transitions. Since only the channels whose Q values lie below the bell-shaped curve can actually occur, it is clear that the only allowed transfers are neutron pick-up and proton stripping. All the other channels are hindered by optimum Q-value consideration. From the same figure we note that for some channels, in particular the two-proton stripping and two-neutron pick-up, the reaction mechanism favors transitions leading to high excitation energies.

These simple findings have been demonstrated in almost all measured systems. An example is shown in figure 7 where we plotted the isotopic distribution of the different charges populated in the indicated reactions [52, 53]. One observes that the strongest channels are those corresponding to the neutron pick-up and proton stripping processes as the optimum

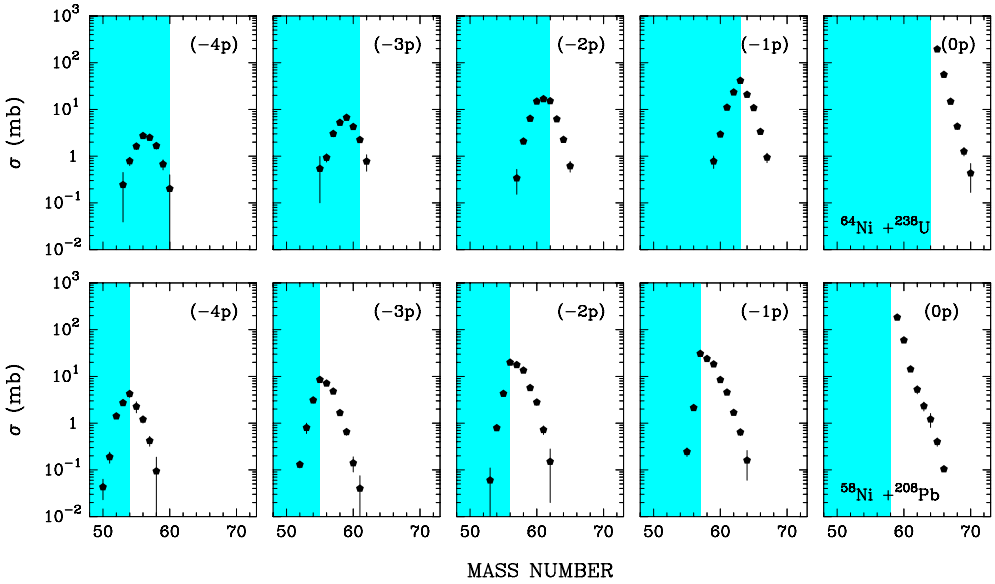

Figure 7. Isotopic distributions for the transfer channels up to the stripping of four protons are shown for the reaction ^{64}Ni+^{238}U at 390 MeV bombarding energy (top) and for the reaction ^{58}Ni+^{208}Pb at 328 MeV bombarding energy (bottom). The shadowed regions mark the transition from neutron stripping to neutron pick-up. Data are from [52, 53].

Q-value rule suggests. It is only for charges far from the entrance channel that one observes sizeable contributions that seems to derive from the stripping of neutrons, this is particularly evident for the collision with uranium where the isotopic distributions peak at masses lighter than the pure proton stripping channels. This should not be a surprise since these channels can be populated via other complicated processes like evaporation, deep inelastic or fission. The situation depicted in figure 7 holds for most of the projectile–target combinations available with stable beams, it is only by employing unstable beams that all the four kinds of basic transitions shown in figure 6 become available.

Concerning the angular momentum transfer we here recall that at low bombarding energies, where the relative velocity of the two ions is much smaller than the intrinsic velocity of the transferred nucleon, the transfer reaction tries to maximize the transferred angular momentum [54], while at high bombarding energies, where the velocity of relative motion is comparable to the intrinsic velocity of the transferred nucleon, the reaction minimizes the transferred angular momentum [55]. This finding may be understood by requiring that the orbitals of the transferred nucleon match smoothly. The semi-classical theory is able to reconcile these two extreme behaviors with a correct treatment of the so-called recoil [56].

3.3. Multinucleon transfer channels

In the near past large efforts, both experimentally and theoretically, have been devoted to the understanding of the transition from a regime of direct reactions (quasi-elastic) to the more complicated regime of deep inelastic. These last processes are characterized by a massive transfer of nucleons (toward the charge equilibration) and very large energy losses. The exit fragments emerge with energies lower than the Coulomb barrier with an angular distribution

that is proper of direct reactions (bell shaped, with a maximum close to the grazing angle). While this last characteristic indicates that the process is very fast the large energy losses indicate that the two ions, before the emerging point, acquire large deformations. These two conflicting findings, short collision time and large energy losses, suggested that in the evolution of the reaction the excitation of surface modes plays an important role being the low-lying modes the main source for the formation of the large deformations.

The exchange of nucleons may constitute the main source for the dissipation of energy as can be understood with a very simple model. Let us suppose to have a system for which N independent single-particle transitions can occur all with the same probability p. In such a system the probability to have the transfer of n particles is simply given by the binomial distribution:

$$P_n = \binom{N}{n} p^n (1-p)^{N-n}. \tag{21}$$

For this distribution the average number of transferred particles is $\langle n \rangle = pN$ so that the corresponding average energy loss is $\langle E_{\rm loss} \rangle = \langle n \rangle Q$. In a heavy-ion collision the number of open channels is very large ($N \sim 100$) so that with $p \sim 0.1$ one estimates an average number of transferred nucleons of the order of 10 and an average energy loss of 50 MeV if for each transition one loses 5 MeV. As this simple example shows, particle transfer may provide the main source for the dissipation of energy.

It was the necessity to have a description of the reaction able to treat at the same time quasi-elastic and deep inelastic events that lead to the development of the reaction code GRAZING [18]. Here we will not attempt to summarize the formalism that is lying behind the model since it can be found in the cited references [16, 17], but we will outline its main ingredients and some of the approximations that have been introduced in the description of the reaction.

The two nuclei are described as an ensemble of independent nucleons that can vibrate around their spherical equilibrium shapes, the basic degrees of freedom being surface vibrations and single particle degrees of freedom. The two ions interact via a Coulomb plus nuclear interaction and may exchange nucleons. For the excitation of the surface modes the model employs the macroscopic approximation whose form factors are proportional to the r-derivative of the ion–ion potential and whose strength are given by the experimental $B(E\lambda)$. The surface modes are treated in the harmonic approximation and to all orders.

The exchange of nucleons is governed by microscopic form factors that take into account the single-particle properties of the two colliding ions. The model, for each transfer mode, stripping and pick-up of neutrons and protons, uses a representative form factor that is parametrized in accordance with [51]. The different single-particle states that are participating to the transfer process are described by introducing average single particle level densities.

The model GRAZING constructs the probability $P(E^*_{\rm a}, E^*_A, N_{\rm a}, Z_{\rm a}, \ldots)$ for a given transition characterized by several observables such as the excitation energy, E^*_i, number of neutrons N_i, number of protons Z_i and so on of the reaction product. This probability is constructed not by solving directly the semiclassical system of coupled equations (9) but by introducing a characteristic function:

$$\begin{aligned} P(E^*_{\rm a}, E^*_A, N_{\rm a}, Z_{\rm a}, \ldots) &= \langle \Psi(t) | \delta(\hat{H}_{\rm a} - E^*_{\rm a}) \cdots \delta(\hat{Z}_{\rm a} - Z_{\rm a}) \cdots | \Psi(t) \rangle \\ &= \int_{-\infty}^{+\infty} {\rm d}\beta_{\rm a}\, {\rm d}\beta_A \cdots Z(\beta_{\rm a}, \beta_A, \ldots)\, {\rm e}^{-{\rm i}E^*_{\rm a}\beta_{\rm a} - i E^*_A \beta_{\rm a} - \cdots} \end{aligned} \tag{22}$$

where the Z function is defined by

$$Z(\beta_{\rm a}, \beta_A, \xi_{\rm a}, \xi_A, \ldots) = \langle \Psi(t) |\, {\rm e}^{{\rm i}\hat{H}_{\rm a}\beta_{\rm a} + {\rm i}\hat{H}_A\beta_{\rm a} + {\rm i}\hat{N}_{\rm a}\xi_{\rm a} + \cdots} | \Psi(t) \rangle \tag{23}$$

$\beta_a, \ldots$ being the parameters introduced ad hoc. For details confer [16, 17]. It is important to mention that the transition probabilities are calculated following classical trajectories constructed in a self-consistent way so as to be compatible with the different quantities defining the final states.

For the description of the relative motion and for the calculation of the inelastic form factors, GRAZING uses the following parametrization of the nuclear ion–ion potential [57]:

$$U_{aA}^{N} = -16\pi\gamma a \frac{R_a R_A}{R_a + R_A}\left[\frac{1}{1 + e^{(r-R_a-R_A)/a}}\right], \tag{24}$$

where the nuclear radii are given by

$$R_i = \left(1.20A_i^{1/3} - 0.09\right) \quad \text{fm}. \tag{25}$$

The diffusion parameter is

$$\frac{1}{a} = 1.17\left(1 + 0.53\left(A_a^{-1/3} + A_A^{-1/3}\right)\right) \quad \text{fm}^{-1} \tag{26}$$

and the surface tension is

$$\gamma = -.95\left[1 - 1.8\frac{(N_a - Z_a)(N_A - Z_A)}{A_a A_A}\right] \quad \text{MeV fm}^{-2}. \tag{27}$$

In the above expression, A_i is the mass number and Z_i, N_i denote the charge and neutron number, respectively. For the Coulomb interaction the model uses the two point charges expression.

Before discussing some application of GRAZING in actual cases it is important to check if its approximations in the treatment of particle transfer, in particular the use of representative form factors for the transfer and the substitution of the actual distribution of single particle states with a density function, are appropriate. To check this we compare in figure 8 the angular distributions of the inclusive (energy integrated) one-particle transfer channels calculated with GRAZING and DWBA calculations done by employing all bound single-particle states above the Fermi energy and a full shell below. The DWBA calculations have been done by using one-particle transfer form factors constructed from the single-particle wavefunctions of the states involved in the transition and by using the WKB approximation for the distorted waves describing the relative motion [4]. Since the WKB approximation has to be employed in a complex potential we name this calculation CWKB [32, 58]. For comparison the experimental data of [32, 53] are also reported.

The reaction of ^{58}Ni on ^{124}Sn constitutes one of the best examples that any model of heavy-ion reaction should confront itself. It is in fact one of the very few cases where for different bombarding energies, most of the channels have been measured in great detail, from elastic scattering, transfer reactions to evaporation residue, deep inelastic and fission products (see [59, 60] and references therein). This reaction has been analyzed within a quantum-mechanical coupled channels frame [60] that includes the excitation of surface modes and the transfer of nucleons. To reduce the number of channels for each inelastic excitation (and single nucleon transfer) the rotating frame approximation of [61] has been used. Of particular interest is the treatment of the transfer degrees of freedom that have been included up to higher order to be able to describe, in the successive approximation, multinucleon transfer channels. A pair transfer using the macroscopic approximation of [62] for the form factor has been also included. Some results of these calculation are shown in figure 9 for the elastic angular distribution and for the neutron transfer channels. With the same model the fusion reaction has been calculated and a good agreement with the experimental data has been found.

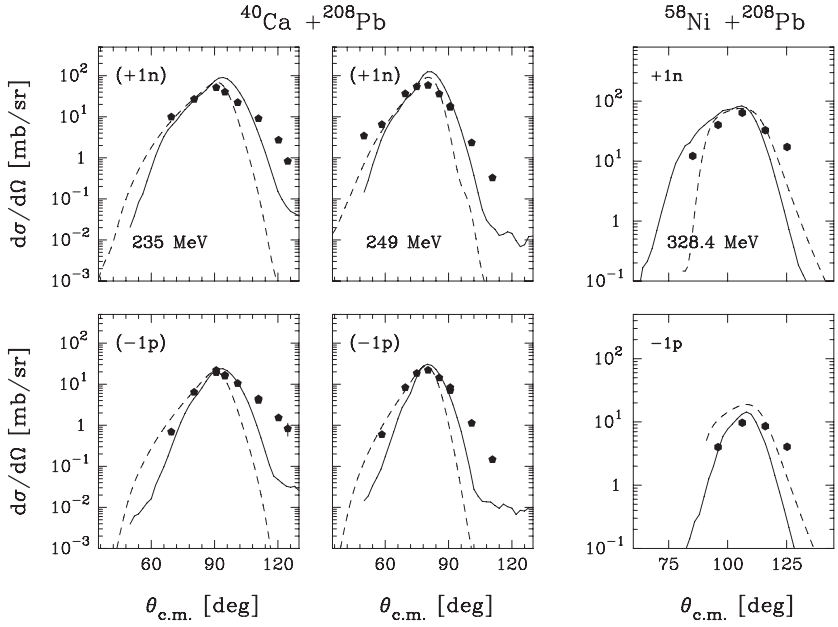

Figure 8. For the indicated reactions and bombarding energies are shown the angular distribution of inclusive one-particle transfer reactions calculated with GRAZING (dash) in comparison with those calculated in the CWKB approximation. The experimental data of [32, 53] are also reported. Note that for these reactions only proton stripping and neutron pick-up are allowed from optimum Q-value arguments, as experimentally observed.

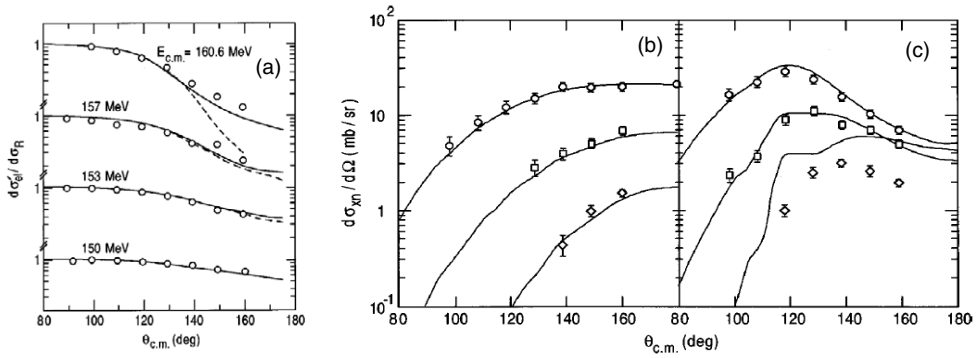

Figure 9. Angular distributions for elastic scattering (a), and +1n, +2n and +3n transfer channels at 150 MeV (b) and 160.6 MeV (c) in the ^{58}Ni+^{124}Sn reaction. Data (circles) are from [59]. (Adapted from [60]).

It is natural to check the ability of GRAZING to describe the reaction by using the data for the same ^{58}Ni+^{124}Sn system. In figure 10, for the indicated bombarding energies, the angular distributions for quasi-elastic, one-neutron pick-up, one-proton stripping and for some multineutron transfer channels [63] are shown. We stress that in these calculations no imaginary part has been added to the potential being the absorption described directly by the

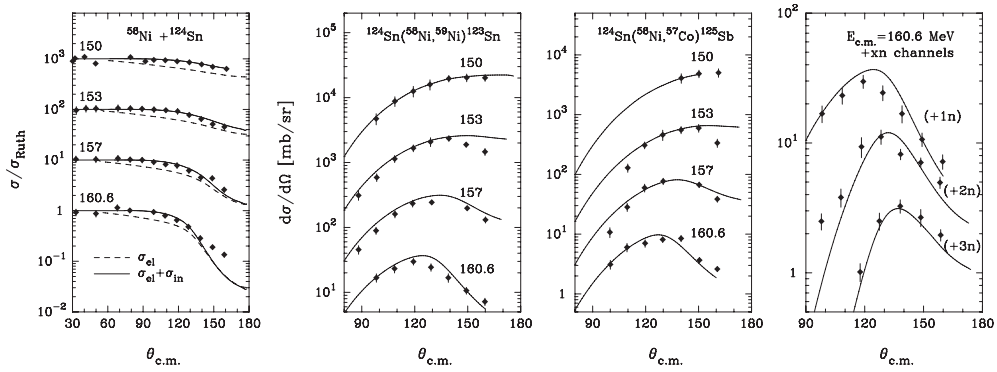

Figure 10. Center-of-mass angular distributions for elastic plus inelastic, one-neutron pick-up, one-proton stripping and some multineutron transfer channels calculated with GRAZING. The label in each frame indicates the center-of-mass bombarding energy in MeV. The data (points) are from [59]. (From [63]).

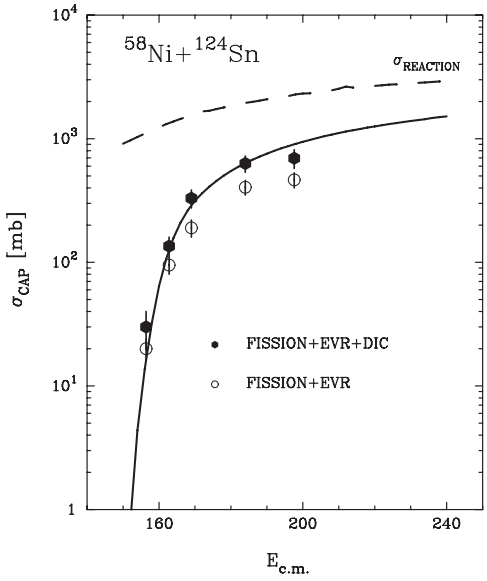

Figure 11. Experimental (points) and GRAZING calculations (lines) for different reaction channels in the ^{58}Ni+^{124}Sn system. The dashed line represents the total reaction cross sections, while the solid line is the sum of evaporation residue (EVR), fission and deep inelastic (DIC) cross sections (capture). (Adapted from [63].)

coupling to the reaction channels. As in all GRAZING calculations for the surface modes one uses the lowest 2^+ and 3^- states and the corresponding giant resonance.

The model is also able to estimate the capture cross section. This is shown in figure 11 in comparison with the experimental data. The good agreement with the data could be obtained only after summing up the deep inelastic components with the evaporation residue and fission ones. This is because GRAZING provides only an estimation of the flux that overcomes the Coulomb barrier but is not able to follow the evolution of the system toward the formation of

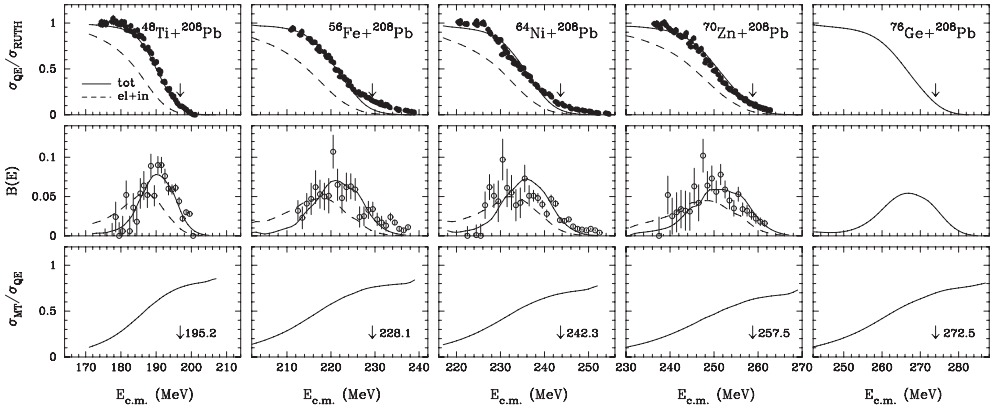

Figure 12. Quasi-elastic excitation function (top), barrier distribution (middle) and ratio of transfer channels to the total quasi-elastic cross section (bottom). All the cross section have been calculated at $\theta_{c.m.} = 172^{\circ}$. The down-arrows represent the Coulomb barrier for the entrance channels calculated with the empirical potential of [4] and using a two points-charge Coulomb potential. The dashed lines are the results considering as quasi-elastic all the final channels belonging to the entrance channel mass partition. The data are from [67]. (From [63].)

a di-nuclear complex and/or to the formation of a compound nucleus. This last comparison clearly suggests that the potential used in the code is quite accurate, we recall that this potential has been derived from a double folding formalism and by fitting the different parameters to give a good description of elastic scattering data.

A further insight on our knowledge of the ion–ion potential and of the mechanism that governs the evolution of the reaction is provided by the barrier distribution concept. In fusion reactions, the effect of the couplings to the intrinsic degrees of freedom of the system can be depicted as giving rise to a smearing over several energies of the Coulomb barrier [64]. These barrier distributions can be extracted from the fusion excitation function by taking the second derivative of the energy weighted fusion cross sections [65]. It has been suggested that a similar information can be derived from the energy dependence of the quasi-elastic cross sections at backward angles [66]. The barrier distribution obtained with these two methods turns out to be in reasonable agreement with each other, although those extracted from quasi-elastic are somewhat broader and with less structure. A recent analysis [63] showed how the barrier distribution obtained from quasi-elastic cross sections depend on what one defines as quasi-elastic. Since quasi-elastic reactions, besides elastic and inelastic channels, receive contributions also from transfer channels (both neutrons and protons), they provide a very interesting tool to investigate the role of transfer reactions in heavy-ion collisions, in fact the importance of transfer channels has always been very elusive from fusion reactions [20, 21].

The experimental excitation functions for various projectile and target combinations in the medium heavy mass region recently measured in [67] are shown in figure 12. Of particular interest here are the results depicted in the third row that show the contribution of the transfer channels, as a function of energy, to the quasi-elastic cross section. It is clear that their contribution grows with the bombarding energy. In the middle row the extracted barrier distributions are depicted. Here to demonstrate the importance of the coupling we report with a vertical arrow the position of the unperturbed barrier. The coupling spreads the barrier in a quite large energy interval. It is seen how the quasi-elastic barrier distribution depends on

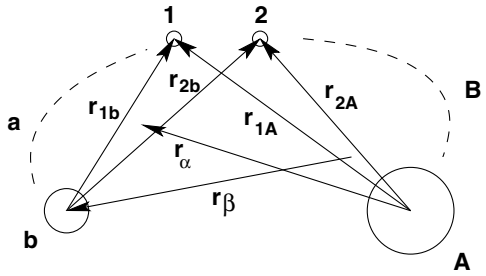

Figure 13. The coordinate system used for the description of the transfer of two nucleons, labeled as 1 and 2. b and A are the cores in projectile-like and target-like.

what we consider as quasi-elastic, so one may expect a difference with respect to the results obtained from the fusion cross sections. It is worth recalling that while what one extracts from fusion reactions [68] reflects how the couplings modify the transmission coefficient, what one gets from quasi-elastic reflects the modification of the reflection coefficient. If fusion and quasi-elastic scattering exhaust most of the total reaction cross section the barrier distributions are expected to be quite similar. However, for heavy systems, where the reaction is dominated by complicated processes like deep inelastic where the nuclei may overcome the Coulomb barrier but separate again with large energy losses and mass transfer, caution must be taken in the interpretation.

3.4. Two-particle transfer

In this subsection, we recall some important aspects of two-particle transfer reactions, these being the reaction of choice for the study of particle–particle correlation in nuclei. For very light ions, the outcome of these reactions has been essential for the formulation of the concept of pairing vibrations/rotations that allowed us to correlate the 0^+ excited states in neighboring even–even nuclei [1].

The first approach for the analysis of these reactions was a simple generalization of the formalism used for one-particle transfer, i.e. the two nucleons were seen as a cluster. In this model, the cluster has a single state as internal motion and it moves in some average potential around the core b (cf figure 13). Of course it was immediately recognized the necessity of a microscopic calculation which includes the coordinates of the individual nucleons. For the case of a pair of nucleons in the states a_1' and a_2' in the projectile that are transferred in the states a_1 and a_2 of the target the transition amplitude may be written as

$$T_{\alpha\beta} = \int \mathrm{d}\vec{r}_\alpha \, \mathrm{d}\vec{r}_{1b} \, \mathrm{d}\vec{r}_{2b} \, \chi_\beta^{(-)*}(\vec{r}_\beta) \langle b, A + (12) | (V_\beta - U_\beta) | b + (12), A \rangle \chi_\alpha^{(+)}(\vec{r}_\alpha) \tag{28}$$

and the form factor may be reduced in the form:

$$\begin{aligned} F_{a_1 a_2, a_1' a_2'} &= \langle b, A + (12) | (V_\beta - U_\beta) | b + (12), A \rangle \\ &= \langle \phi^{a_1}(\vec{r}_{1A}) \phi^{a_2}(\vec{r}_{2B}) | [V(\vec{r}_{1A}) + V(\vec{r}_{2A})] | \phi^{a_1'}(\vec{r}_{1b}) \phi^{a_2'}(\vec{r}_{2b}) \rangle. \end{aligned} \tag{29}$$

With $V(\vec{r}_{iA})$ we have indicated the single particle shell model potential (of the target) that is felt by the nucleons of the projectile and which is responsible for the transfer. The structure of the matrix element for the transfer of two nucleons is easily seen in the no recoil approximation ($\vec{r}_\alpha = \vec{r}_\beta$). In this approximation, the above matrix element assumes the following form:

$$F_{a_1 a_2, a_1' a_2'} = \langle \phi^{a_1} | \phi^{a_1'} \rangle \langle \phi^{a_2} | V | \phi^{a_2'} \rangle + \langle \phi^{a_1} | V | \phi^{a_1'} \rangle \langle \phi^{a_2} | \phi^{a_2'} \rangle. \tag{30}$$

This expression shows clearly that the matrix element derives from the product of an overlap term (the two bases used to write the transition amplitude (28) are in fact non-orthogonal) times the matrix element of the one-particle transfer. If several shell model pairs (a_1a_2) contribute to the wavefunctions of initial and final states the form factor becomes a sum over many two-particle form factors arising from the various initial and final state two-nucleon configurations, i.e. it should be written as

$$F = 2 \sum_{12,1'2'} B^{(b)}(a'_1a'_2)B^{(A)}(a_1a_2)\langle\phi^{a_1}|\phi^{a'_1}\rangle\langle\phi^{a_2}|V|\phi^{a'_2}\rangle \tag{31}$$

where the B coefficients are the so-called two-particle spectroscopic factors representing the amplitudes of a given pure configuration in the total wavefunctions that is obtained by diagonalizing, in the pure two-particle configurations, the residual interaction responsible for the particle–particle correlation.

Here we do not intend to summarize all the work that has been done for the inclusion of the recoil in the evaluation of the amplitudes but we just want to recall that the above formalism, while adequate for the reproduction of the shape of the angular distributions, has serious problems in the description of the magnitude of the measured cross section for two-nucleon transfer processes. This inadequacy prevented the use of these reactions (at least with heavy ions) to gain direct information on pair correlation in nuclei. Bayman pioneered the discussion of this problem, not only developing a Monte Carlo method for the calculation of the transfer amplitude where the recoil term was exactly taken into account, but pointing out that the amplitude (28) represents just the simultaneous contribution to the transfer process [69]. The successive mechanism is in fact missing in the above expression. Here we prefer to discuss this essential point by using a semiclassical formalism since it is simpler to implement and to understand. Following [69, 70], the semiclassical amplitude for the transfer of two nucleons from channel $\alpha \equiv (a(=(b+12), A)$ to channel $\beta \equiv (b, B(=A+12))$ may be written in the form:

$$a^{(2)}_{\beta\alpha} = a^{(\mathrm{sim})}_{\beta\alpha} + a^{(\mathrm{seq})}_{\beta\alpha} + a^{(\mathrm{orth})}_{\beta\alpha}. \tag{32}$$

The first term corresponds to the simultaneous (first order) transfer of a pair, the second one to the sequential transfer and the last term arises from the non-orthogonality of the bases used to describe the two mass partitions. As at the beginning of this section, we write the three components considering pure configurations $(a'_1a'_2)$ and (a_1a_2) in the entrance and exit channels, respectively, and we neglect the angular momentum couplings. Here it suffices to remember that the treatment of angular momentum implies the addition of a contribution proportional to the third component of the transferred angular momentum to the exponential phase.

For the simultaneous term one has

$$a^{(\mathrm{sim})}_{\beta\alpha} = -\frac{2\mathrm{i}}{\hbar}\int_{-\infty}^{+\infty} \mathrm{d}t\; f^{a_1a'_1}(r(t))g^{a_2a'_2}(r(t))\,\mathrm{e}^{\mathrm{i}\varsigma_{\beta\alpha}(t)} \tag{33}$$

while for the sequential:

$$a^{(\mathrm{seq})}_{\beta\alpha} = -\frac{\mathrm{i}}{\hbar}\sum_{i,j} C^A(a_i)C^b(a'_j)\int_{-\infty}^{+\infty} \mathrm{d}t\; f^{a_ia'_j}(r(t))\,\mathrm{e}^{\mathrm{i}\varsigma_{ij}(t)}\int_{-\infty}^{t} \mathrm{d}t'\, f^{a_ja'_i}(r(t'))\,\mathrm{e}^{\mathrm{i}\varsigma_{ji}(t)} \tag{34}$$

and the non-orthogonality term is

$$a^{(\mathrm{orth})}_{\beta\alpha} = \frac{2\mathrm{i}}{\hbar}C^A(a_i)C^b(a'_j)\int_{-\infty}^{+\infty} \mathrm{d}t\; f^{a_1a'_1}(r(t))g^{a_2a'_2}(r(t))\,\mathrm{e}^{\mathrm{i}\varsigma_{\beta\alpha(t)}}. \tag{35}$$

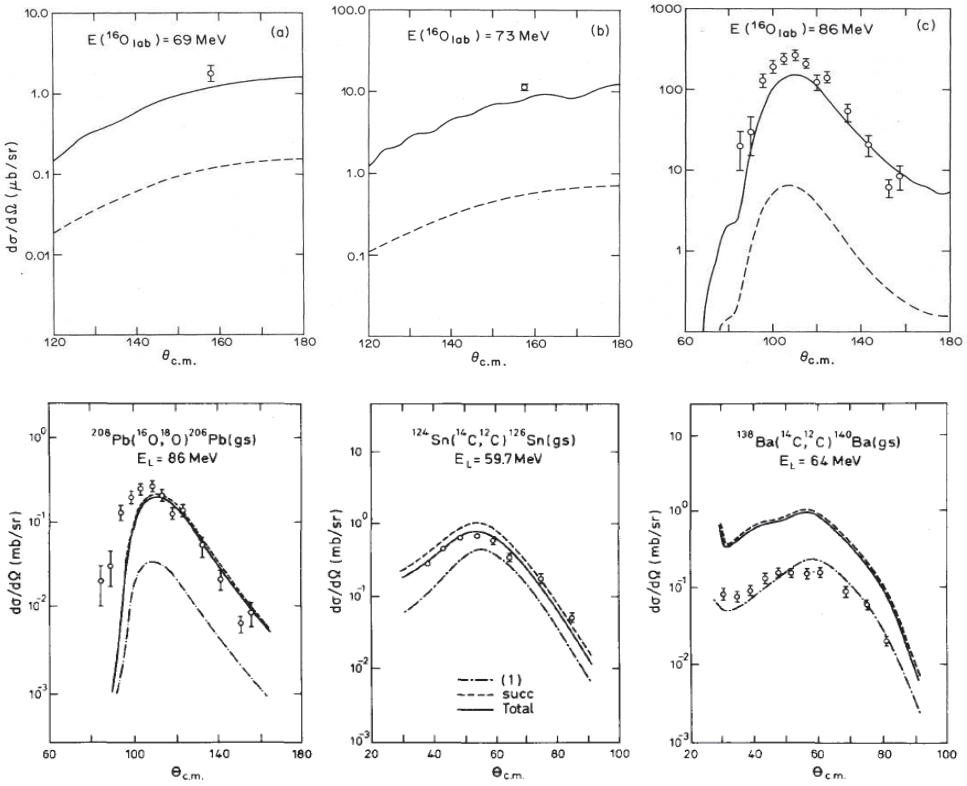

Figure 14. Angular distributions for two-nucleon transfer reactions (points are the experimental data). In the top row the quantal results of [69] are shown for the ^{16} O+^{208}Pb system, where the first two frames refer to energies below the Coulomb barrier. The bottom row shows the semiclassical results of [70]. The contribution of the successive components clearly dominates the cross sections (adapted from [69, 70]).

In the above expressions in order to shorten the notation we introduced the phase:

$$\varsigma_{\beta\gamma} = -\frac{1}{\hbar}(E_\beta - E_\gamma)t + \gamma_{\beta_\gamma}(t). \tag{36}$$

The label γ in the above expression represents the final channel β in the simultaneous and non-orthogonality term while it is the intermediate channel $\gamma \equiv (c = (b + 1), C = (A + 1))$ in the successive term; with f we have indicated the single particle form factors as defined in equation (11) while with g we have indicated the overlap matrix element. It is derived from the expression for the one-particle form factor putting to unity the interaction.

In figure 14, some examples of two-neutron transfer reactions analyzed within the above formalism are reported and compared with experimental data. In the first row the results from the quantum-mechanical calculations of [69] are shown, while the bottom row shows the semiclassical calculations of [70]. In all the shown cases it is seen that the contribution of the successive mechanism dominates the cross section. This finding does not mean that the two-particle spectroscopic factors extracted by using the one-step formalism (simultaneous) has to be doubted. In fact, it has been seen that the relative contributions of the two mechanisms do not depend on the different states populated by the transition, so that the relative spectroscopic factors are not altered. What the results mean is that the successive

mechanism not only dominates the two-nucleon transfer but all multinucleon transfer channels are probably dominated by the same successive mechanism.

The formalism we have just outlined for the calculation of the two-nucleon transfer matrix element implies a microscopic description, in that the initial and final states are described as a superposition of the elementary components that in this case are two single particle states. The weight of the different components results from the diagonalization of the residual interaction responsible for the correlations. In [62], it has been suggested that also for this process one can identify a collective variable that characterizes it by following an analogy between the pairing vibrations and the more familiar surface oscillation.

Assuming the saturation of the nuclear densities, the acquisition or loss of two nucleons is achieved by changing the nuclear volume, which implies a displacement of the nuclear surface. The transition density associated with this pair mode may be easily calculated by identifying ΔA as the macroscopic pairing variable so that

$$\delta\rho^P = \frac{\partial\rho}{\partial A} = \left(\frac{R_0}{3A}\right)\frac{\partial\rho}{\partial r}\Delta A, \tag{37}$$

where ρ is the nuclear density and R_0 is the half-density radius. As in the case of the inelastic excitation, the form factor for this mode becomes

$$F^P(r) = \beta_P\left(\frac{R_0}{3A}\right)\frac{\partial U(r)}{\partial r}, \tag{38}$$

where $U(r)$ is the optical potential. The scaling factor β_P, obtained by normalizing the theoretical calculation to the experimental data, may be interpreted as the strength of the pair mode. Of course this formalism for the description of the pair-transfer mode requires some crucial steps that may be quite controversial and of not a too easy acceptability. One of them is the introduction of a particle–particle local transition density and its use in the context of a one-body operator (the shell model potential of the other nucleus) to calculate the form factor via a folding prescription. A lot of theoretical work has been done in order to elucidate the above points (cf [4]) but very little could be achieved until now in establishing a certain systematics over the values of the pairing deformation parameter β_P.

The formulation of the pairing vibrations/rotations model received a substantial contribution from extensive transfer data obtained with light ions, primarily with (p, t) and (t, p) reactions [1–3]. These reactions are dominated by transitions that populate the 0^+ ground states for targets away from the shell closure while populate 0^+ excited states for targets close to the shell closure. The strength of these transitions has been characterized by an enhancement factor of the order of 30 with respect to a two-particle unit of cross section [1], introduced, in analogy to the Weisskopf unit for inelastic transition, to characterize these transfer cross sections. As a two-particle unit of cross section one takes the largest cross section calculated in distorted wave Born approximation (DWBA) for a pure two-particle configuration.

In heavy-ion collisions, it is very difficult to discriminate the population of individual states (by particle detection only) and it is difficult to use the same enhancement factor to characterize the two-particle transfer reactions. Nevertheless one has been trying to look at the problem by defining an enhancement factor by using directly the experimental data [7, 30, 71]. This can be done by exploiting the fact that at low energy the transfer cross section can be written as a product of the elastic cross section times the transfer probability $P_{\rm tr}(\theta)$, i.e.:

$$\left(\frac{{\rm d}\sigma}{{\rm d}\Omega}\right)_{\rm tr} = \left(\frac{{\rm d}\sigma}{{\rm d}\Omega}\right)_{\rm el} P_{\rm tr}(\theta). \tag{39}$$

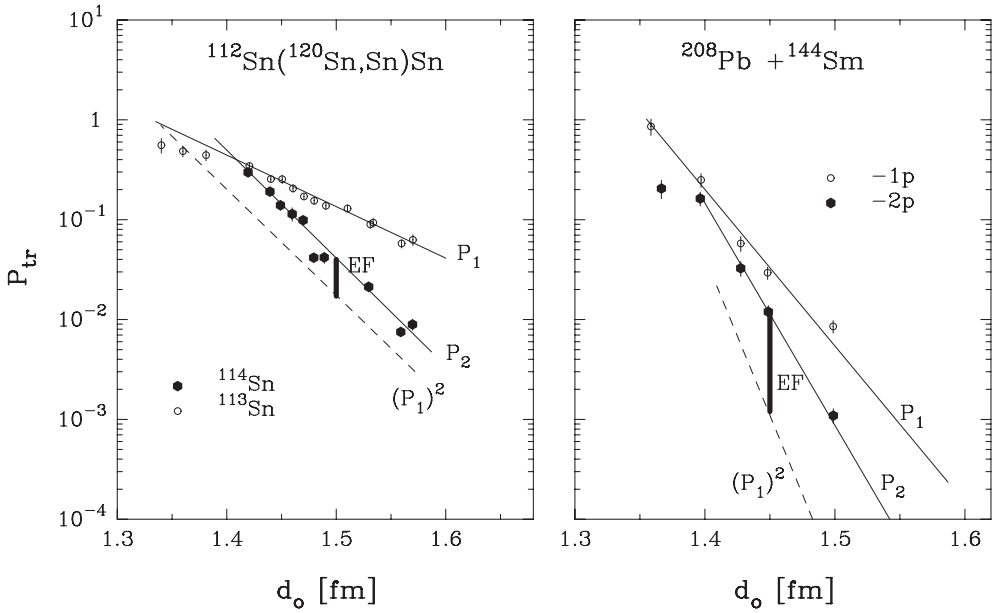

Figure 15. The one- and two-particle transfer probabilities as a function of the overlap distance d_0 are shown for the indicated reactions. The straight line is drawn to indicate the exponential decay of the cross section (adapted from [30]).

Since the form factor for transfer decays exponentially and the main contribution to the probability comes close to the turning point $R_{\min}(\theta)$ of the classical trajectory leading to the scattering angle θ, one may write

$$P_{\rm tr}(\theta) \simeq {\rm e}^{-2\kappa R_{\min}(\theta)} \tag{40}$$

with $R_{\min}(\theta)$, for a Coulomb trajectory, given by

$$R_{\min}(\theta) = \frac{Z_{\rm a} Z_A e^2}{2E}\left(1 + \frac{1}{\sin\theta/2}\right). \tag{41}$$

In the above expression, the parameter κ is related to the binding energy of the transferred 'cluster'. To be able to superimpose on the same graph several systems it is customary to plot the transfer probability as a function of the parameter:

$$d_0(\theta) = \frac{R_{\min}(\theta)}{A_{\rm a}^{1/3} + A_A^{1/3}}. \tag{42}$$

In a semi-logarithmic plot the excitation functions (or angular distributions) of transfer processes are thus represented by straight lines with a slope -κ.

If P_1 is the probability for the transfer of a single nucleon, in a particle independent model we can write for the transfer of two nucleons the expression (cf equation (21)):

$$P_2(d_0) = [P_1(d_0)]^2. \tag{43}$$

Now, P_1 may be extracted directly from the experimental data as in figure 15 so that for the two-particle transfer we obtain the prediction represented by the dashed line in the same figure. By normalizing this prediction to the experimental data one extracts the desired enhancement factor. In the cases of figure 15 these factors are of the order of ∼3 for neutrons and of the

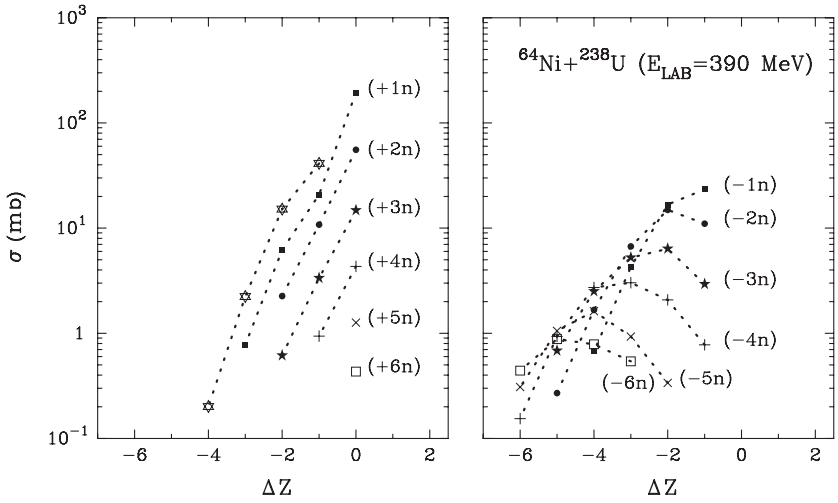

Figure 16. Experimental total cross sections as a function of the number of transferred protons ΔZ for channels involving neutron pick-up (left panel) and neutron stripping (right panel) in the indicated reaction. To guide the eye we connected, with dashed lines, the different proton transfer channels corresponding to an equal number of neutrons (adapted from [52]).

order of ∼10 for protons (note that for protons the predicted two-proton transfer cross section has a slope that is not parallel to the data, thus the value of the enhancement factor becomes questionable).

The data shown in figure 15 are inclusive, i.e. integrated over all Q values. This fact makes it difficult to ascribe the found enhancement factors to the effect of the two-particle correlations induced by the residual interaction. This is because the residual interaction does not alter the value of the sum rule but redistributes the total strength among few collective states. The found enhancement factors have to be most likely ascribed to the reaction mechanism being more complicated that the one implied by equation (43), for instance a direct contribution of a pair transfer. Quite recently the same procedure has been used in exclusive data obtained via γ-particle coincidences [46, 72], and enhancement factors of the order of 1000 have been reported (see also the following section).

3.5. Evaporation

In analyzing the yields of multinucleon transfer reactions it is very important to realize that secondary processes like evaporation can alter considerably the isotopic distribution of the yields. It is possible, from a simple analysis of the experimental data of inclusive cross sections, to show that several mechanisms, besides the direct process, are at work in defining the final distribution.

To this purpose, one plots the total cross sections as a function of the number of transferred protons (ΔZ), as is done in figure 16 for the ^{64}Ni+^{238}U system [52]. On the left-hand side of this figure we display the cross sections involving neutron pick-up, while on the right-hand side the ones involving neutron stripping. As it is apparent from this plot the neutron pick-up and neutron stripping reactions have a very different behavior. The neutron pick-up decreases in a very smooth way as the number of transferred protons increases, while neutron stripping reactions have a much more erratic behavior. This is a clear indication that these two kinds

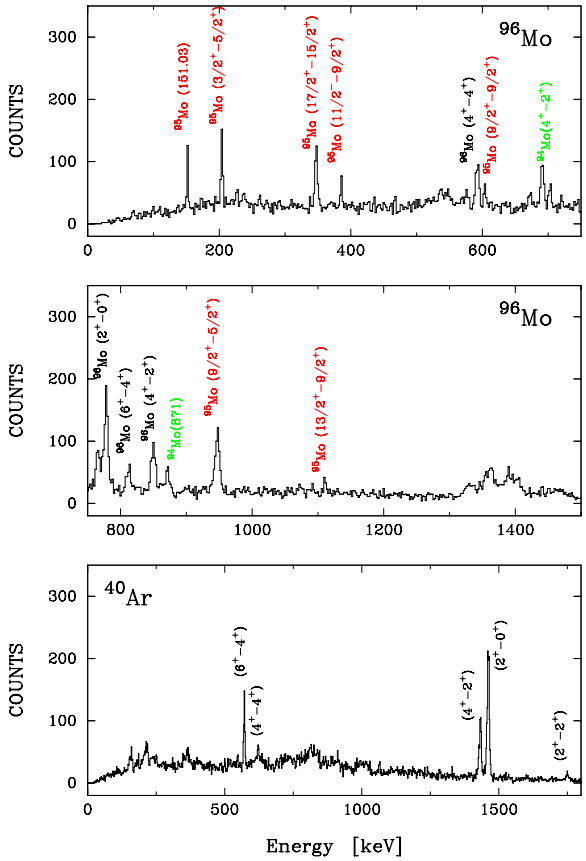

Figure 17. γ spectra for the $-2p + 2n$ channel in the reaction ^{40}Ca+^{96}Zr at $E_{lab} = 152$ MeV Doppler corrected for the (undetected) heavy (top two frames) and light fragments (bottom frame). The ^{96}Mo labels refer to the primary binary fragment. To have a better identification of the different γ lines for the heavy fragment we used an expanded energy scale (from [41]).

of final states are populated by different mechanisms. While the neutron pick-up behavior indicates a direct population in terms of independent transfer of neutrons and protons the neutron stripping side shows that the yield of these reactions depends on a more complicated mechanism. They are much more influenced by neutron evaporation, in fact, from optimum Q-value arguments one knows that neutron stripping reactions are strongly hindered.

This kind of behavior has been seen in all studied reactions, both with light and heavy systems, indicating that in the transfer process large amount of energy is exchanged between projectile and target. Part of this excitation energy is dissipated by evaporation, in particular neutrons. It is this process that predominantly populates the lighter isotopes of a given nuclear species.

In γ-particle experiments, by identifying in Z and A the light partner of the binary reaction with a spectrometer, one detects not only its coincident γ lines but also those associated with the heavy binary partner and its neighboring nuclei that can be populated via evaporation. An example is shown in figure 17 where for the reaction ^{40}Ca+^{96}Zr we show the γ-spectra of ^{40}Ar together with those of Mo isotopes, properly Doppler corrected. In the γ spectrum of the

Mo-like nuclei lines belonging to different isotopes are identified, those of ^{96}Mo are populated from the direct reaction while those of the lighter Mo isotopes are most likely coming from nuclei populated via neutron evaporation.

It is clear that to have a quantitative comparison with theory, the calculated yields must be corrected for evaporation, these processes are particularly relevant for studying nuclei far from the entrance channel.

3.6. Production of heavy neutron-rich nuclei

We have seen that with stable beams only proton stripping and neutron pick-up are likely to occur in transfer processes. As a consequence target nuclei tend to gain some charge while loosing neutrons, a mechanism that populates nuclei to the left of the stability valley. We have previously seen that this feature of transfer reactions is embedded in the optimum Q-value rule, that, for the characteristic behavior of the binding energy, is essentially governed by the lighter partner of the reaction. It is only by taking heavier isotopes of a given projectile that a transition to the opposite situation should occur [8].

The amount of neutron excess needed for the production of neutron-rich isotopes and the isotope dependence of the yield can be estimated with the semiclassical code GRAZING that has been illustrated above. Some results are shown in figure 18 for the collision of Xe beams on ^{208}Pb target at 700 MeV of center-of-mass energy. The figure shows clearly that with neutron-rich projectiles one may populate nuclei not too far from the target but with fewer charges and more neutrons. The figure shows the production yield corrected by neutron evaporation, this process clearly works against the production of very neutron rich nuclei.

4. Presentation of the data

At the end of the previous section, it has been suggested that multinucleon transfer reactions may provide a useful tool for the production of heavy neutron-rich nuclei. In this section, we will present multinucleon transfer data on different systems that are analyzed in the semiclassical framework illustrated above. Of course, these studies are of more general character, for instance, they are important for discerning the role of transfer channels in defining the barrier penetration (fusion reactions and quasi elastic barrier distribution), for studying the transition from the quasi-elastic regime to the more complex deep inelastic processes and they may reveal the existence of degrees of freedom that are not incorporated in the above model.

Here we recall once more that GRAZING calculates the distribution of yields among the different reaction channels by including surface degrees of freedom (low-lying 2^+ and 3^- states of projectile and target) and the exchange of nucleons (neutrons and protons) treated independently and in the successive approximation from the single particle transfer.

4.1. Inclusive cross sections

In figure 19, we display the measured isotopic yields for the reaction ^{64}Ni+^{238}U [52], in comparison with calculations. The data have been obtained by integrating the differential cross sections in an angular range close to the grazing angle so that the plotted cross sections represent the direct population of the different mass yields. These yields for the small charge transfers are peaked around the mass corresponding to the pure proton stripping, while for larger charge transfers it is observed a drift toward lighter isotopes. This last fact has been ascribed in the

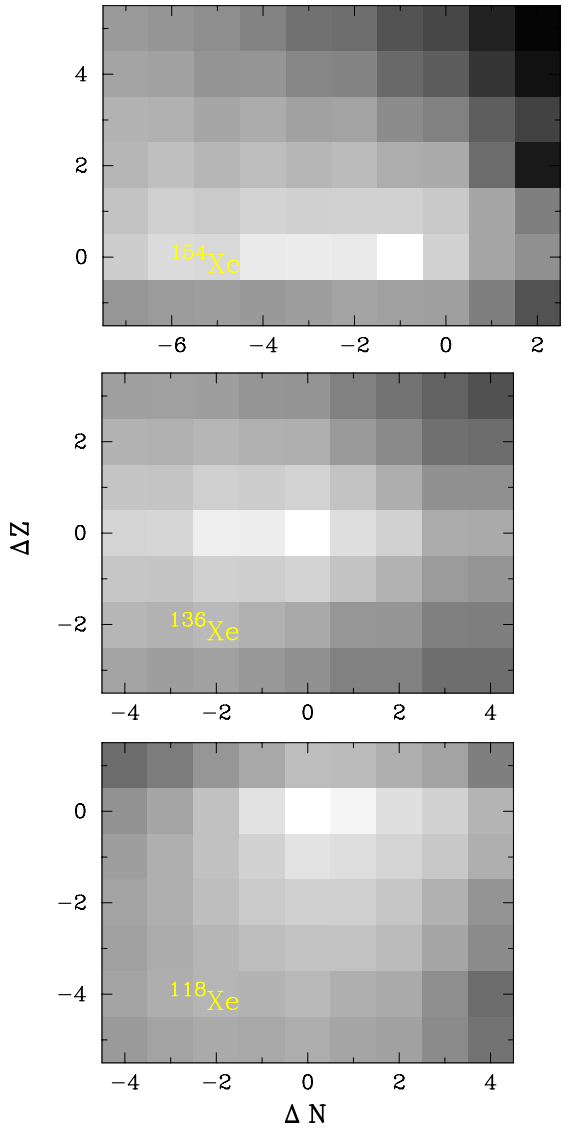

Figure 18. Production yields of multinucleon transfer reactions as a function of ΔN and ΔZ. The results refer to the collision of Xe isotopes on ^{208}Pb at 700 MeV of center-of-mass bombarding energy.

previous section to the influence of evaporation. The theory describes reasonably well the pure neutron transfer and the $(-1p)$ isotopes but underestimates considerably all the other charges. However, we stress that GRAZING accounts correctly for almost 80% of the direct transfer yield. For the explanation of the discrepancies at large charge transfers, it is very difficult at this stage to say what is missing in the model, as degrees of freedom or as reaction mechanism.

The same problems have been observed in all systems measured so far. As a further example, in the top row of figure 20 we show the equivalent results for the ^{58}Ni+^{208}Pb system.

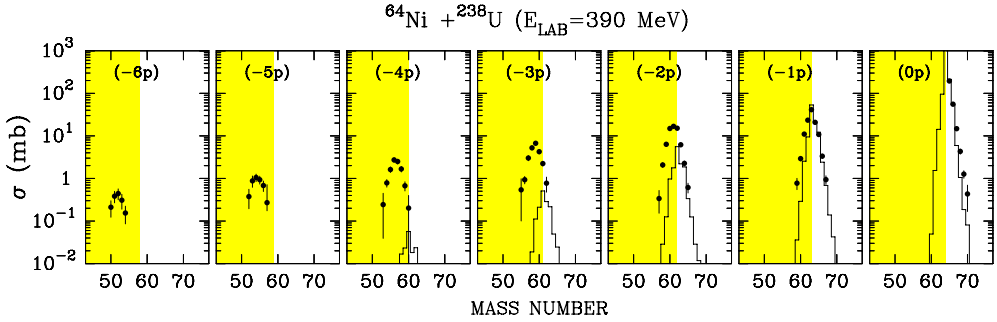

Figure 19. Total cross sections for the different isotopes (as a function of mass) populated in the reaction ^{64}Ni+^{238}U at $E_{\rm lab} = 390$ MeV in comparison with the prescription of the semiclassical model GRAZING (histograms) (adapted from [52]).

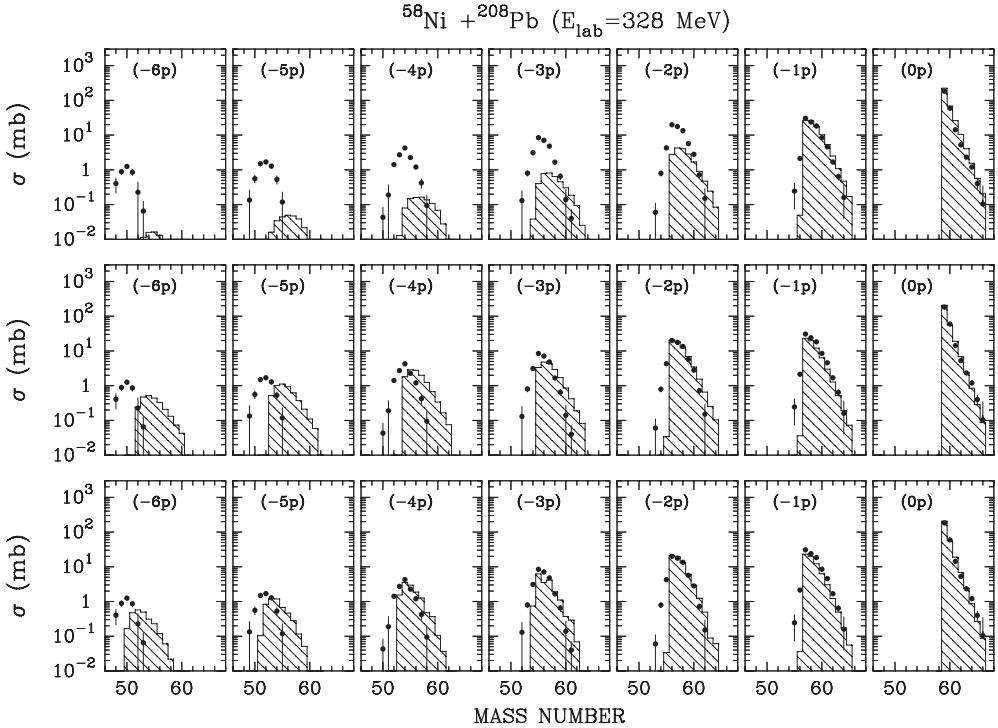

Figure 20. Total cross sections for the transfer channels observed in ^{58}Ni+^{208}Pb. Points are the experimental data while the histograms are the results of calculations taking into account independent particle transfers (top row), the addition of pair modes for neutrons and protons (middle) and neutron evaporation (bottom) (from [53]).

Here we note that the shape of the yield distribution reflects very nicely the optimum Q-value rule that for stable nuclei favors neutron pick-up and proton stripping. The bell shapes are only restored for massive charge transfers. In the process to understand the charge distribution we tried to add in the calculation the contribution of a direct pair mode both for neutrons and protons, by using the macroscopic formulation. To keep at minimum the number of

parameters we choose to add a single pair mode placed at the optimum Q-value and we used the strength of the form factor (kept the same for neutrons and protons) to fit the pure -2p channel. The results of such a calculation are shown in the middle row of the figure. Since the model provides the excitation energy of the single fragments we are in condition to correct the primary yield for the evaporation process, the final yield distributions are shown in the bottom row of the figure where now a reasonable overall description is obtained, note that this has been achieved by using a single parameter, the strength of the form factor for pair mode.

Unfortunately, the code GRAZING does not allow us to add other degrees of freedom of the two ions in the calculations, the model includes the surface modes (low-lying and high-lying 2^+ and 3^- states) and the single particle transfer via an average form factor (for neutrons and protons, stripping and pick-up) and a density of single particle states. To include the pair mode one has to use another code, based on the CWKB approximation. Its main characteristics are that for the single particle transfer it uses the actual distribution of single particle levels that are coupled with the true form factors (it has been developed to check the different approximations that are included in the GRAZING program). The multinucleon transfer is obtained via a successive mechanism that mimic the approximation of GRAZING. For the relative motion the program uses the WKB approximation and it is constructed to reproduce the ordinary DWBA calculations for the one-particle transfer channels (for more details see [32]).

The role of the pair mode is seen more clearly in figure 21 where for the two indicated systems we display the inclusive cross sections for pure neutron and pure proton transfer channels. Note that the pair mode alters very little the cross section for neutron transfer but is essential for the proton transfer. Here we would like to stress that the pure one-neutron pick-up is much larger (almost a factor 10) with respect to the pure one-proton stripping transfer. This may mask the effect of the pair mode since the successive mechanism gives a much larger contribution for neutrons than for protons.

The angular distribution provides an important information on the reaction mechanism that is behind the transfer process. In figure 22, we show the angular distributions (Q-value integrated) for some transfer channels for the reaction ^{58}Ni+^{208}Pb. The bell shape of these distributions is an indication of the direct nature of the underlying process. The theoretical description, both in shape and in the position of the grazing angle, demonstrates the correctness of the used nuclear potential and the chosen range of partial waves that contribute to the cross sections. The theory on the other hand underestimates considerably the yield at large total kinetic energy loss as is shown in figure 23. Again, this may indicate that more complicated processes populate the given isotopes and that the theory most likely underestimates the reshuffling in the final distributions due to neutron evaporation. One should also stress that the experimental TKEL has been constructed by assuming a binary reaction therefore the shapes of the distributions may be somewhat altered, especially for massive transfer channels.

The available inclusive data on neutron transfer show that the total angle and Q-value integrated cross sections for pure neutron transfer channels drop by an average factor of $\simeq$3.5–4 per each transferred neutron suggesting that the process in question proceeds via a successive transfer of independent particles. One may argue that a possible contribution from neutron pair modes could show up as an odd–even staggering in the mass yields. However in inclusive transfer data, as it has been suggested in the previous section, it is very difficult to see this effect since the total transfer yield is not modified by the residual interaction that is responsible for the pair correlations. To study this aspect the system ^{62}Ni+^{206}Pb has been investigated [73]. This system has been chosen since the ground–ground state Q values for pure neutron transfer are all close to optimum Q-value ($Q \simeq 0$) and equals within 1–2 MeV, furthermore the even isotopes of lead form a system of pair vibration and the energies

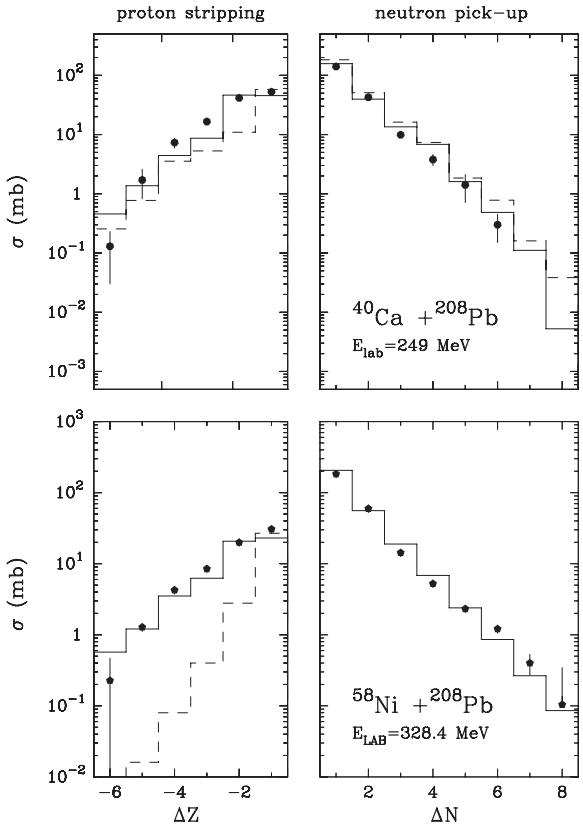

Figure 21. Total cross sections (points) for pure neutron pick-up (right frames) and pure proton stripping (left frames) channels for the ^{40}Ca+^{208}Pb and ^{58}Ni+^{208}Pb systems. The dashed lines are the results of calculations with only independent particle transfers, the full lines include in addition a pair transfer mode for both neutrons and protons and take into account the effect of the evaporation (adapted from [32, 53]).

of their 2^+ levels are all very similar, within 150 keV, and constitute a nice example of quadrupole pairing states. These properties of lead nuclei should favor the population of levels close to the ground states and eventually should enhance the effect of the transfer of pairs [71].

In figure 24, we show the experimental Q-value integrated differential cross sections obtained at an angle close to the grazing as a function of the number of transferred neutrons. The measurement has been done at three bombarding energies to see if and how these pair modes persist as a function of the excitation energy. To show any possible odd–even staggering the data points have been connected with lines, one for the odd-transferred channels and the other for the even. The trend of the data is almost energy independent and, at least within the experimental accuracy, displays a constant drop of the cross sections as a function of the transferred number of neutrons without any clear odd–even staggering, the one-neutron pick-up channel seems, at all energies, to have a somewhat lower cross section than that suggested by the common trend. The results obtained in these inclusive measurements seem to indicate that multineutron transfer channels are dominated by a sequential mechanism.

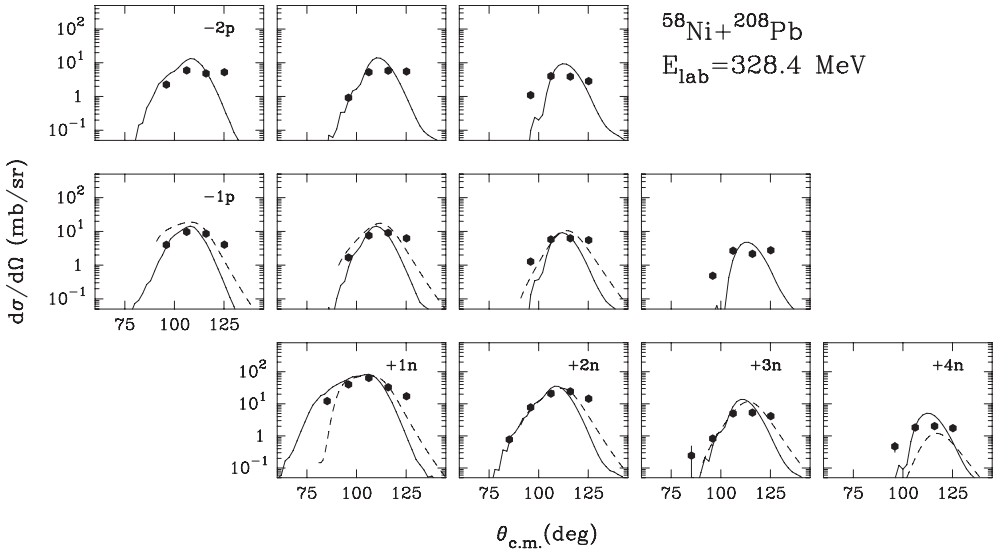

Figure 22. Experimental (dots) Q-value integrated angular distributions for transfer channels in the ^{58}Ni+^{208}Pb reaction at $E_{\rm lab} = 328.4$ MeV. The solid and dashed lines are the calculations done with the CWKB and GRAZING, respectively (from [53]).

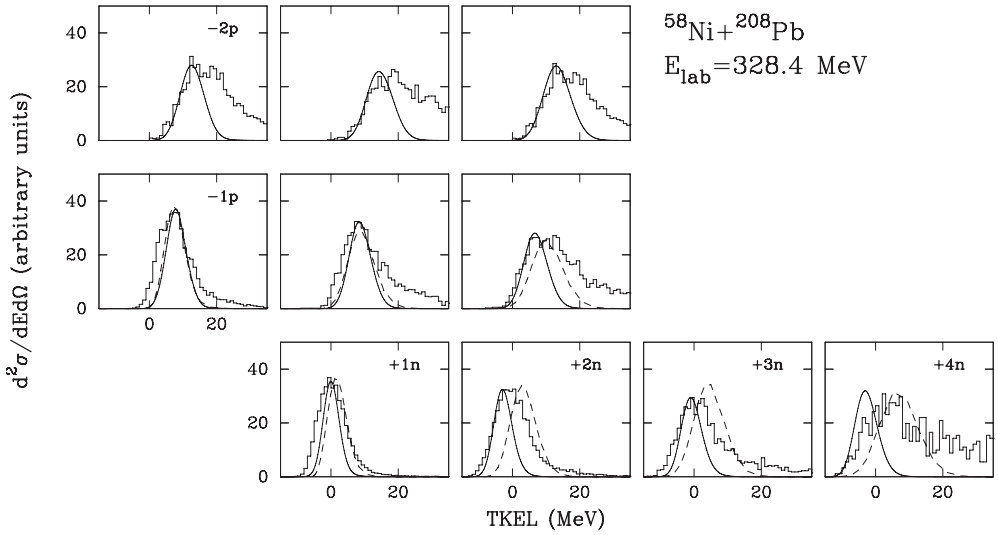

Figure 23. Experimental (histograms) total kinetic energy loss distributions at $\theta_l = 90^o$ for transfer channels in the ^{58}Ni+^{208}Pb reaction at $E_{\rm lab} = 328.4$ MeV. The solid and dashed lines are the calculations done with the CWKB and GRAZING, respectively (from [53]).

An interesting question is to what extent this observed behavior of neutron transfer yields at near barrier energies persists in the sub-barrier domain. Here the two ions probe their mutual interaction only at very large distances, where the nuclear couplings are dominated by transfer processes. The number of open reaction channels is obviously reduced, the Q-value distributions get narrower, thus simplifying the study of the reaction. However,

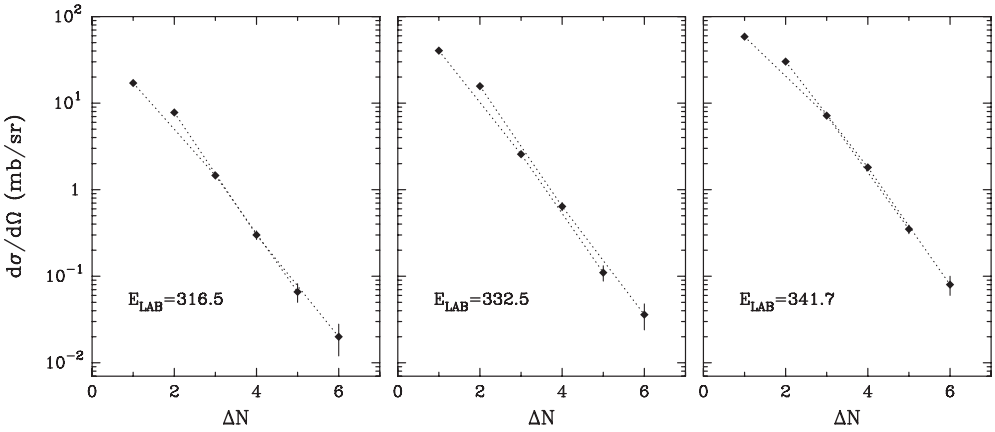

Figure 24. Experimental differential cross sections for pure neutron pick-up channels in ^{62}Ni+^{206}Pb at the indicated bombarding energies as a function of the number of transferred neutrons (ΔN). The dotted lines are a guide for eye and connect the even and odd ΔN (from [73]).

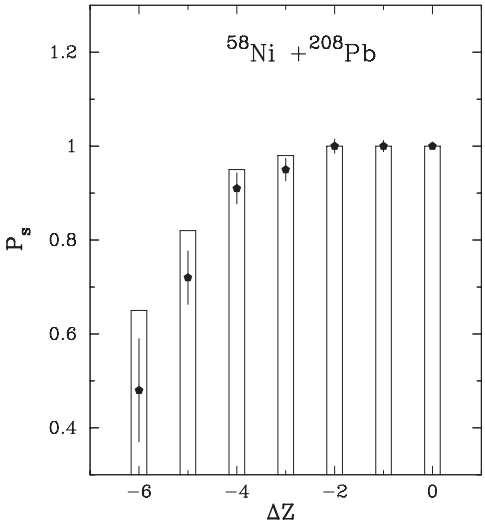

Figure 25. Survival probability against fission P_s for the heavy target-like fragments produced in the ^{58}Ni+^{208}Pb reaction at $E_{\rm lab} = 328$ MeV as a function of the number of transferred protons ΔZ detected with a spectrometer averaged over neutron numbers. Points and histograms are the experimental and theoretical values, respectively (from [53]).

measurements of heavy-ion transfer reactions at sub-barrier energies are very scarce due to significant technical difficulties [29]. New possibilities are presently offered with large solid angle spectrometers, and very recently the inverse kinematic technique at far sub-barrier energies has been employed with the PRISMA spectrometer for the study of multineutron and multiproton transfer channels in the ^{94,96}Zr+^{40}Ca systems.

To finish this section, we want to say some words about the survival probability of the heavy partner since it is for this fragment of the reaction that the multinucleon transfer mechanism may be of relevance for the production of neutron rich nuclei. In addition to

evaporative processes, the heavy fragments may be affected by fission. To check the relevance of these processes, besides the light transfer products identified with a spectrometer, the heavy reaction partners have been detected in kinematic coincidence by using position sensitive gas detectors at the proper geometry [53]. This (simple) technique is valid if the velocity of the recoils before fission is small compared to that of the fragments after fission so that the fission products are smoothly distributed in position and can be easily subtracted from the peak of the coincident heavy recoils. In this way, from the experimental ratios between coincidences of light and heavy binary partners and the light ones detected with the spectrometer, we could obtain the survival probability against fission (P_s) of the heavy fragments for the ^{58}Ni+^{208}Pb system, as shown in figure 25 for each (mass integrated) Z. Also in this case we compared the obtained results with the semiclassical calculations. The semiclassical distribution in mass, charge, energy and angular momentum has been used as input for the code PACE [74]. The observed good agreement is a further support for the used model. This study has been performed with stable beams, but, with some caution, it may be a reasonable basis for more general studies with radioactive beams.

4.2. Pair mode

In the above section, we have seen that to have a reasonable agreement with the inclusive data one had to include the contribution from a pair mode but we have also seen that it is very difficult to have a clear signature of this mode solely from inclusive data. In searching for possible signatures of these pair modes, studies have been pursued on neutron pick-up channels in closed shell nuclei, the ^{40}Ca+^{208}Pb system [75]. In the left panel of figure 26 we show the TKEL distributions measured at $E_{\rm lab} = 236$ MeV for channels up to +4n in comparison with theoretical predictions. One observes that the spectra display a well-defined maxima at energies higher than the ground–ground state Q values (indicated by the down-arrow) so that, besides for the +1n, the reaction leaves unpopulated the ground states (we recall that the optimum Q-value for all neutron transfer channels is close to zero).

The calculation gives an overall good description of the experimental spectra and by looking at the final population of the single particle levels one could infer that the maxima are dominated by transitions that deposit neutrons in the $p_{3/2}$ orbital of the Ca nuclei. This, for the ^{42}Ca, is compatible with the excitation of 0^+ states at $\simeq$6 MeV as it is shown in the right panels of figure 26 where for the +2n channel the TKEL distributions measured at three bombarding energies are displayed. We note here that the spectra widen with the increase of the bombarding energy with a slight shift of the maxima reflecting the energy dependence of the optimum Q-value and that the reaction seems to favor the population of the 0^+ states at 6 MeV of excitation energy.

In trying to understand the origin of this concentration of strength at 6 MeV of excitation energy a large-scale shell model calculation [76] has been performed for this nucleus to extract the strength distribution of the 0^+ states. This theoretical distribution is shown in the bottom right panel of figure 26. A strong concentration near $\sim$6 MeV of excitation energy is clearly seen, this is very close to the energy of a configuration where a $p_{3/2}$ neutron pair is coupled to the ^{40}Ca ground state. From the illustrated facts it is tempting to suggest that the maxima in the TKEL spectra correspond to the excited 0^+ states that were identified with a pair mode in [1]. Using ^{48}Ca as the ground state of the pair vibrational model these states are here interpreted as the mode (4, 1) in ^{42}Ca and (4, 2) in ^{44}Ca, the numbers in parentheses refer to the pair-removal ($n_{\rm r}$) and to the pair-additional ($n_{\rm a}$) mode, respectively.

A direct confirmation of the above suggestions may come by looking at the decay modes of ^{42}Ca by means of particle-γ coincidences. In figure 27, we show the γ-spectrum obtained

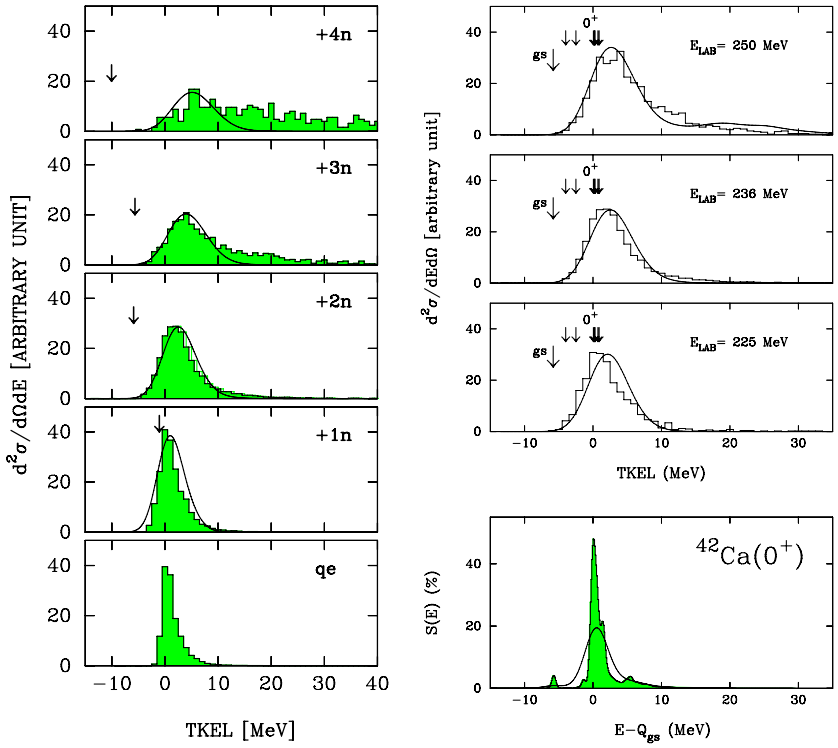

Figure 26. Experimental (histograms) and theoretical (curves) total kinetic energy loss distributions for quasi-elastic (qe) and neutron pick-up channels at $E_{\rm lab} = 236$ MeV (left side) and for the two-neutron pick-up channels at the three indicated energies (right side). Arrows indicate the ground-to-ground state Q-value. The short arrows on the right frame correspond to the energies of 0^+ states in ^{42}Ca with an excitation energy lower than 7 MeV. The bottom panel shows the strength function $S(E)$ from SM calculations (adapted from [75]).

in the reaction ^{40}Ca+^{96}Zr [41], where projectile-like nuclei have been identified with the PRISMA+CLARA setup. We observe here (see the expanded region) a γ-transition at 4340 keV which is consistent with a decay from a level at 5.8 MeV to the 2^+_1 state. Its angular distribution shows an isotropic pattern, though the limited statistics and the lack of γ–γ coincidences prevents to draw definite conclusions about the spin.

The ^{206}Pb+^{118}Sn system has been recently investigated [46, 72] with the main aim of trying to identify pair transfer effects through searching for enhancement factors as outlined in figure 15 of the previous chapter. This projectile and target combination has characteristics equivalent to those of ^{62}Ni and ^{206}Pb nuclei discussed above, namely ground state Q-values quite similar for pure neutron transfer channels and close within few MeV to the optimum Q-value ∼0. Nuclei have been identified via their characteristic γ decays, and, by requiring multiplicity zero with a coincident filter detector, one could essentially derive the transfer yield to the first excited levels of final nuclei. In figure 28, we show the deduced transfer probabilities as a function of the overlap parameter that is related to the distance of the closest approach for a Coulomb trajectory leading to the scattering angle θ. At variance with the results shown in figure 15, the probability for two-neutron transfer is much larger than the square of the one-neutron transfer probability, as it turns out by extracting the transfer yield for specific excited states.

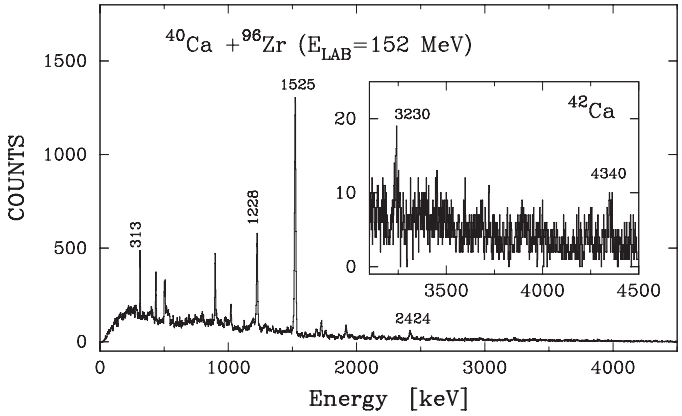

Figure 27. γ-ray spectrum with expanded region in inlet for ^{42}Ca obtained in the ^{40}Ca+^{96}Zr reaction (from [41]).

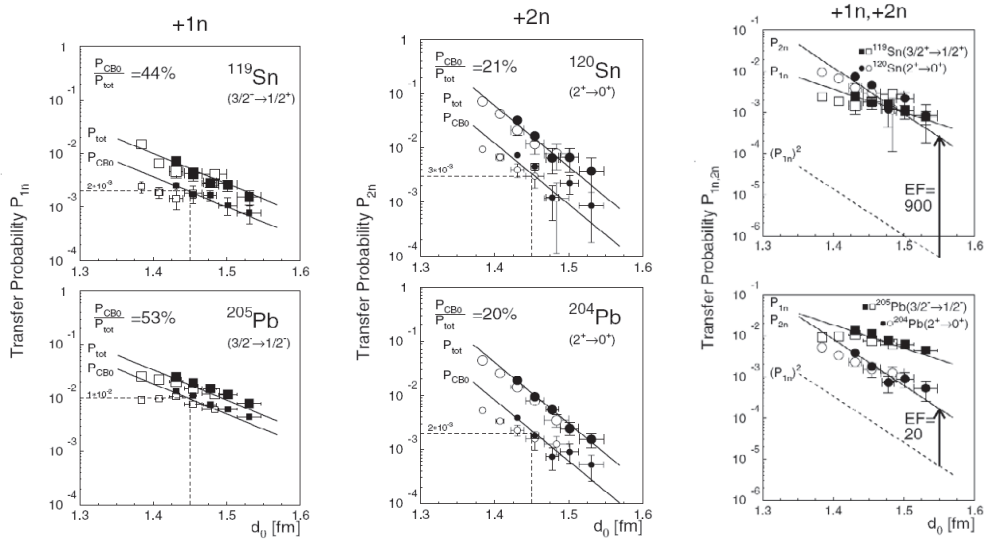

Figure 28. Transfer probabilities as a function of the overlap parameter d_0 for one- and two-neutron transfer channels populated in the ^{118}Sn+^{206}Pb reaction (adapted from [46, 72] which we refer for details).

4.3. Transfer reactions and γ-particle coincidences

Multinucleon transfer reactions have been studied not only with spectrometers (magnetic or time of flight) but also by employing large γ arrays. With these setups the different products of the reaction are identified by their characteristic γ transitions, therefore one can extract the transfer strength to specific excited states but one cannot obtain information about transitions reaching the ground state. By employing position information from particle detectors one can construct the angular distributions for some specific transitions (for instance, from the low-lying states of target and projectile) and then use the Coulomb excitation to get the absolute

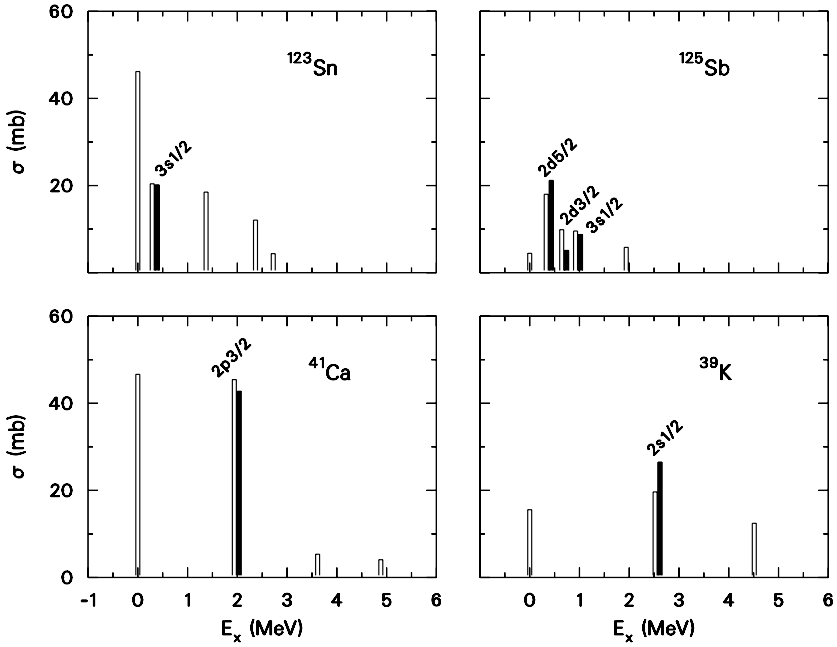

Figure 29. Experimental (full bars) and theoretical (open bars) total cross sections for the +1n (^{41}Ca and ^{123}Sn) and −1p (^{39}K and ^{125}Sb) channels populated in the ^{40}Ca+^{124}Sn at $E_{\rm lab}$ = 170 MeV. For the ^{123}Sn the line at zero excitation energy includes the population of the metastable state at 24.6 keV. The cross section to this state accounts for more than 80% of the total flux. The absolute value for cross sections was obtained by normalizing the intensity of the lowest $2^+ \rightarrow 0^+$ transition of ^{124}Sn to a DWBA calculations (from [47]).

normalization (transformation from counts to mb). Via γ–γ coincidences one can construct the spectra of the interested nuclei and thus extract information about the excitation energy range that can be reached in these reactions.

The population to individual final states for the ^{40}Ca+^{124}Sn system has been achieved by employing a γ-particle coincidence technique, identifying the transfer products through their characteristic γ transitions [47]. Doppler correction has been applied once for the light and once for the heavy partners, and the contribution of the feeding from higher-lying states has been taken into account to obtain for the different single particle states (reached in one-neutron pick-up and in one-proton stripping) the total cross sections plotted in figure 29. These data have been compared with calculations done in the spirit of the CWKB to check the single-particle form factors, the results are shown in the same figure. Note how the calculated ground–ground state cross sections (which could not be extracted from such an experiment) for one-neutron transfer channels (for both ^{41}Ca and ^{123}Sn) represent a substantial fraction of the total +1n yield.

We mentioned several times that with heavy-ions, even with the use of magnetic spectrometers, it is very difficult to discriminate between individual states and that only inclusive cross section can be determined. The use of γ-array detectors may in principle help in this task (at least for some systems) but we are missing here the possibility to measure the ground-state transitions. Here we would like to illustrate an interesting possibility, offered by the coupling of a magnetic spectrometer (PRISMA) with the large γ array (CLARA) for the determination of elastic scattering in a heavy-ion collision.

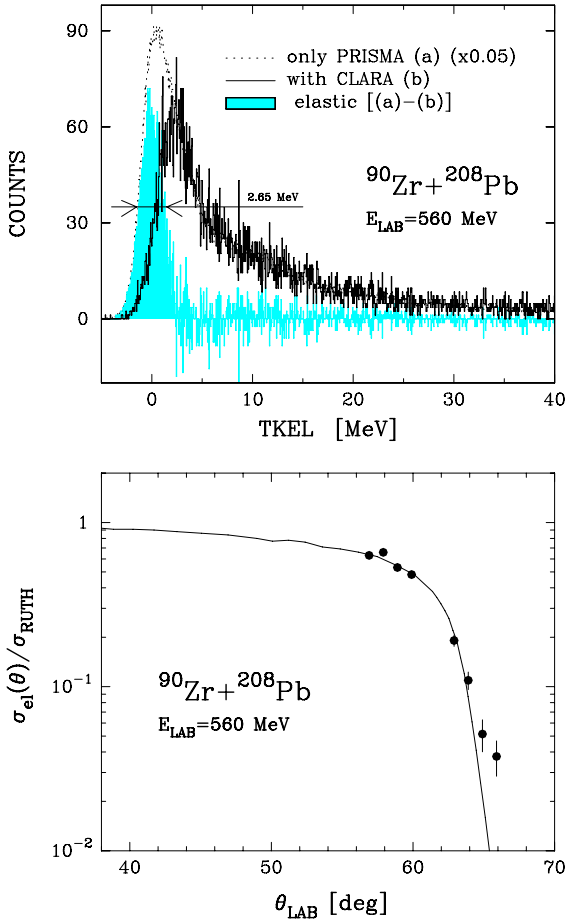

Figure 30. Top: experimental angle integrated total kinetic energy loss distributions (TKEL) for ^{90}Zr in the ^{90}Zr+^{208}Pb reaction (a) without coincidence with γ rays and (b) with at least one γ ray. The two spectra are normalized in such a way that the high TKEL tails match. The gray area corresponds to the subtraction between the two spectra [(a)-(b)], giving a peak whose width is ∼2.65 MeV. Bottom: experimental (points) and GRAZING calculated (curve) differential cross section for elastic scattering, normalized to Rutherford (from [41]).

With this setup the pure elastic scattering is determined by comparing the events with and without γ coincidences. In the top panel of figure 30, the total kinetic energy loss (TKEL) spectra for ^{90}Zr in the ^{90}Zr+^{208}Pb reaction with and without γ-coincidence are shown, normalized in the tail (large TKEL) region. By subtraction, we obtain the contribution of pure elastic (this procedure may not work at angles much forward than the grazing angle since in this region there are only very few γ coming from the inelastic excitation, mostly through the Coulomb interaction, of the first low-lying states). This subtracted spectrum is characterized by a narrow peak centered at TKEL $\simeq$0 MeV with a FWHM of 2.65 MeV. Moreover, its centroid is separated by 2.15 MeV from the maximum of the TKEL spectrum in coincidence with CLARA, whose value is very close to the inelastic excitation of the first 2^+ state in ^{90}Zr. Such a procedure should be reliable, provided that the shape of the spectrum in coincidence with γ rays only weakly depends on the γ multiplicity.

By repeating this subtraction in steps of one degree over the entrance angular range one obtains the elastic angular distribution whose ratio to Rutherford is shown in the bottom panel of figure 30, in comparison with the results of GRAZING calculations. The very pronounced fall-off of the elastic cross section for large angles indicates that the elastic scattering for this system is dominated by strong absorption and the good agreement between theory and experiment tells us that the used potential is appropriate for the reaction and that the reaction channels included in the calculation provide the right depopulation of the entrance channels (absorption). We feel that the use of particle-γ coincidences to determine the true elastic of quite heavy systems is an interesting example of the application of the technique. Of course it has to be tried for other systems and in other conditions, at several bombarding energies and at more forward angles where the number of γ is small. This procedure may indeed provide a very useful tool for the determination of the true elastic also for very heavy systems thus giving important information on the optical potential.

It has been remarked several times that to analyze the experimental yields we have used a model that explicitly treats the internal degrees of freedom of the two ions in terms of elementary modes, surface vibrations and single particles. These modes not only describe the low energy spectra of projectile and target but provide the building blocks for the description of neighboring nuclei. Heavy-ion collisions should provide the ideal tool for the studies of the particle-vibration coupling scheme; in fact, it is through the excitation of these elementary modes that energy and angular momentum are transferred from the relative motion to the intrinsic degrees of freedom and that mass and charge are exchanged among the two partners of the collision. The spectra of the neighboring nuclei, populated in the reaction, comprise partly single-particle or single hole states and partly states that involve combinations of singe-particle or hole with a collective boson.

Of particular importance from this point of view is the contribution of [77] where, in an experiment with thick target, they identified for several nuclei close to ^{208}Pb transitions that evidentiated the coupling of the 3^- state to single particle configurations populated in the reaction and provided matrix elements that are essential for the development of shell model calculations in the particle-vibration coupling scheme. Here we recall that the ^{208}Pb nucleus constitutes an ideal laboratory for the study of particle-phonon states, its first excited states being the collective 3^- at 2.62 MeV and its first positive parity state being the 2^+ at 4.05 MeV. The collectivity of the 3^- is not dominated by few particle-hole components but derives from the cooperative action of many configurations.

In this section, we would like to concentrate on the spectra of the target-like nuclei populated via one-nucleon transfer reactions in the ^{40}Ca+^{96}Zr collision [41]. Our analysis will follow closely that of [77, 78] where the particle-phonon states in ^{209} Bi and ^{207}Pb populated in deep-inelastic heavy-ion collisions have been analyzed in great detail. The ^{96}Zr nucleus presents a more complicated situation, its low-energy spectrum is dominated by a 2^+ state at 1.75 MeV and by a 3^- state at 1.897 MeV. This at last is very collective (51 W.u.) and decays predominantly via an E1 transition through the 2^+ state but has a collective branching via an E3 transition to the ground state. The decay pattern is illustrated in figure 31 where a schematic representation of the levels of ^{96}Zr, ^{95}Zr and ^{97}Nb is depicted. In figure 32, the corresponding γ-ray spectra, obtained by applying Doppler correction for target-like binary partners of ^{40}Ca, ^{41}Ca and ^{39}K detected in PRISMA are reported, respectively.

The ground state of ^{95}Zr is well described by a neutron–hole in the $(d_{5/2})^{-1}$ orbital. By coupling this hole state with 3^-, one expects a sextuplet of states $(1/2^-, 3/2^-, \ldots, 11/2^-)$ at an energy close to that of the 3^- and similarly by coupling the same hole state to the lower 2^+ one expects a quintuplet $(1/2^+, 3/2^+ \ldots, 9/2^+)$ at an energy close to that of the 2^+. The reaction mechanism does not populate the components of the two multiplets uniformly

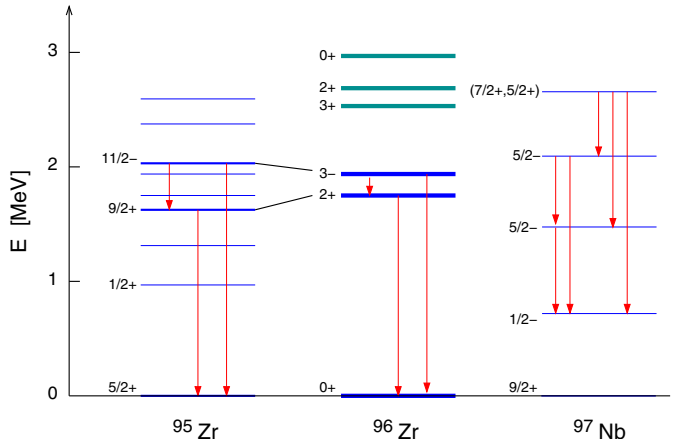

Figure 31. Simplified level scheme of the first excited states of ^{96}Zr, ^{95}Zr and ^{97}Nb. With vertical lines the γ transitions are indicated that are discussed in the text.

but favor the stretched configurations $11/2^-$ and $9/2^+$ since the transfer probability has its maximum at the largest angular momentum transfer. From the adopted levels of ^{95}Zr, the state at 2025 keV populated in (p, d) and (^{3}He, α) reactions (recognized as $9/2^-$, $11/2^-$) is a natural candidate for the stretched configuration $|3^-, (d_{5/2})^{-1}\rangle$. Very recently, the level scheme of ^{95}Zr has been re-measured [79] in heavy-ion induced fission reactions and, the sequence of γ rays of 229.7 [$11/2^- \rightarrow (9/2^+)$], 115.8[$(9/2^+) \rightarrow (7/2^+]$ and 1676.8 $\left[(7/2^+) \rightarrow 5/2^+_{g.s.}\right]$ keV has been proposed for the decay of the $11/2^-$ state. In figure 32, the measured spectra of ^{95}Zr show very clearly all these transitions. In addition, it is visible that a new transition at $E_\gamma = 2022$ keV can be naturally interpreted as the decay to the ground state of the $11/2^-$. The intensity of this transition, relative to the E1, is very similar to that observed in ^{96}Zr thus reinforcing our interpretation that the $11/2^-$ state is a member of a hole-boson $|3^-, (d_{5/2})^{-1}\rangle$ multiplet.

Of course, we would like to look for a similar configuration in the proton sector i.e. in the spectra of ^{97}Nb that is populated in the reaction via a proton stripping process. Here the ground state of ^{97}Nb is quite well described by a pure proton in the $g_{9/2}$ orbital and from the particle-vibration coupling we should expect two multiplets coming from the coupling of the $g_{9/2}$ proton with the 2^+ and the 3^- bosons of ^{96}Zr. Also for the proton stripping channels the population of the two multiplets should be mostly concentrated in its stretched configuration $15/2^-$ for the coupling with the 3^- and $13/2^+$ for the coupling with the 2^+. For this nucleus the adopted level scheme is of little use since the two stretched configuration have not yet been identified. In our spectra, cf figure 32, where the E3 transition is expected, we see two γ rays with energies of 1931 and 2088 keV that can be tentatively proposed for the E3 decay from the $15/2^-$ state (a 2092 keV level is tabulated as $3/2^+$,$5/2^+$). The signature of the E1 decay branch of this $15/2^-$ to the $13/2^+$ member of the multiplet with the 2^+ would require γ–γ coincidences which, within the limit of the accumulated statistics, could not be achieved in the present experiment. However, we observe an intense γ-line at 803.4 keV that is quite close ($E_\gamma = 824.7$ keV) to the $(13/2^+ \rightarrow 9/2^+_{g.s})$ transition in ^{95}Nb identified in recent high spin studies [80]. Thus, placing the $13/2^+$ state at 803 keV, the missing E1 transition from $15/2^-$ could be identified with the very intense transition that we observe at 1276 keV. If this identification is correct we have to place the energy of $15/2^-$ at 2088 MeV. The fact that our

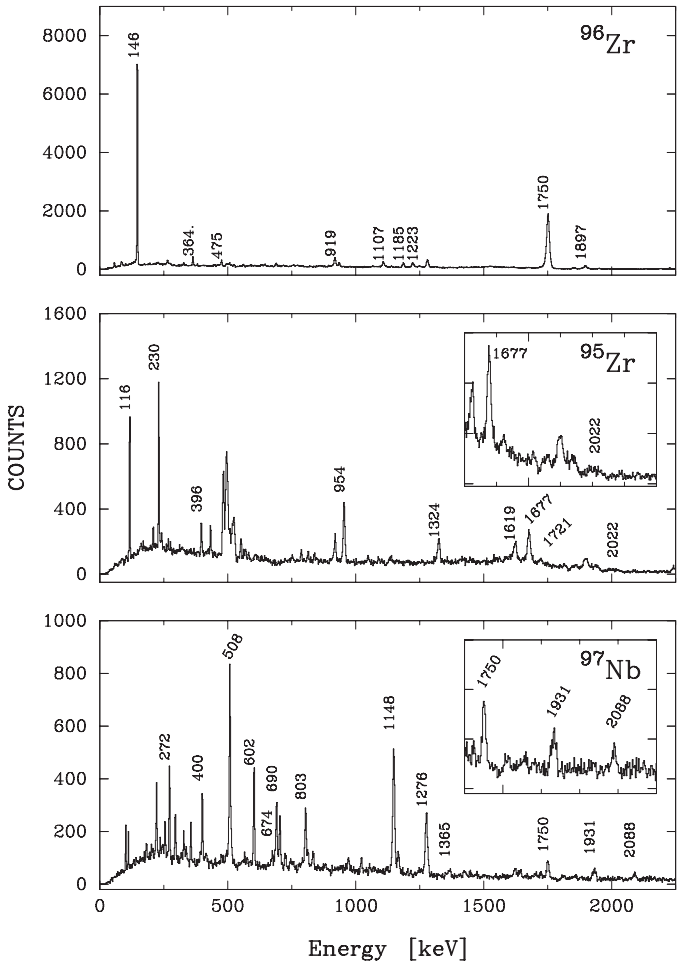

Figure 32. γ-ray spectra for ^{96}Zr, ^{95}Zr and ^{97}Nb obtained in the ^{40}Ca+^{96}Zr reaction (adapted from [41]).

identification places the $13/2^+$ member of the multiplet $|2^+, g_{9/2}\rangle$ at a very low energy should not be surprising since the blocking of the $g_{9/2}$ orbital strongly modifies the wavefunction of the 2^+ states. As mentioned above a clear identification of the decay scheme will require a γ–γ coincidence experiment.

5. Summary and outlook

In this review, we discussed the progress made in the last years in the field of heavy-ion transfer reactions at the Coulomb barrier. Charge and mass yields, differential and total cross sections, and total kinetic energy loss distributions, have been measured for inclusive multineutron and multiproton transfer channels for several systems. The experimental yields have been analyzed with semiclassical theories developed to calculate at the same time quasi-elastic and deep-inelastic processes. These theories have been able to provide a consistent description

of transfer and fusion reactions by using few degrees of freedom, surface modes and single particles.

From the comparison between data and theory, one could probe the importance of the elementary modes in transfer processes and to what extent they can describe the complex mechanism of multinucleon transfer. For the inclusive data, one can presently obtain a reasonable agreement by adding the contribution of a pair mode (simultaneous transfer of a pair of nucleons) that turned out to be of particular importance for multicharge transfer channels. It has been also shown that the direct experimental signatures of these pair modes solely from inclusive cross sections are not conclusive, calling for the discrimination of the final states reached via the transfer process. Also, the theoretical description of these pair degrees of freedom lacks and much more work should be done both from the structure point on view and from the mechanism underlying the transfer of the pair. These studies will be of particular relevance for the foreseen experiments with radioactive beams where the pair correlation should play a relevant role. Effects of particle evaporation due to large energy losses, present even at near barrier energies, have been identified, both indirectly (asymmetric behavior of neutron pick-up and neutron stripping channels) and directly (by exploiting γ-particle coincidences). The effect of particle evaporation and transfer-induced fission of the heavy transfer products has been discussed, being their effects essential for the cross section predictions of neutron-rich (heavy) nuclei produced via multinucleon transfer.

New opportunities are offered by the implementation of large acceptance spectrometers based on trajectory reconstruction. With these devices one gained more than an order of magnitude in the total efficiency while keeping good resolution for the detection of heavy-ion transfer products. Therefore, in coupling them with γ arrays, one can study the transfer yield to specific final states and their decay modes. First studies of this kind together with results of elastic scattering and of the population pattern of states of particle-vibration character have been presented. These results show also that future steps require an increase of the overall efficiency, in order to be able to implement γ–γ–particle coincidences (to unambiguosly identify nuclear structure observables, spin, parity and correctly attribute the levels to a definite nucleus) and to detect high-energy γ rays (important for the decay modes of pairing vibrational structures and other high-lying 0^+ states). Significant improvements in the field can only come by a much wider investigations in different systems, where a complete set of observables is necessary. Very poorly investigated areas are those at sub-barrier energies where nuclei enter into contact through the long tail of the nuclear densities. It is in these regions that, for very neutron-rich nuclei, information on nucleon–nucleon correlation could be obtained simply by studying the excitation functions of specific transfer channels.

Finally, transfer reactions are known to be important in connection with near-barrier studies, where it is mandatory to coherently describe the partition of the total reaction cross sections amongst all open reaction channels, this is particularly delicate for heavy systems where deep inelastic and/or quasi-fission components set-in even at very low energies. Below the barrier, coupling effects on fusion cross sections due to transfer are still an open question and possible improvements may come from detailed studies where elastic, inelastic and transfer channels are unambiguously identified.

References

[1] Broglia R A, Hansen O and Riedel C 1973 *Advances in Nuclear Physics* vol 6, ed M Baranger and E Vogt (New York: Plenum) p 287
[2] Bes D R, Broglia R A, Hansen O and Nathan O 1977 *Phys. Rep* **34** 1
[3] Igarashi M, Kubo K and Tagi K 1991 *Phys. Rep.* **199** 1

[4] Broglia R A and Winther A 1991 *Heavy Ion Reactions* (Redwood City, CA: Addison-Wesley)
[5] Reisdorf W 1994 *J. Phys. G: Nucl. Part. Phys.* **20** 1297
[6] Rehm K E 1991 *Annu. Rev. Nucl. Part. Sci.* **41** 429
[7] Wu C Y, von Oertzen W, Cline D and Guidry M 1990 *Annu. Rev. Nucl. Part. Sci.* **40** 285
[8] Dasso C H, Pollarolo G and Winther A 1994 *Phys. Rev. Lett.* **73** 1907
[9] Broda R 2006 *J. Phys.* G: Nucl. Part. Phys. **32** R151
[10] Otsuka T, Suzuki T, Fujimoto R, Grawe H and Akaishi I 2005 *Phys. Rev. Lett.* **95** 232502
[11] Stefanini A M *et al* 2002 *Nucl. Phys.* A **701** 217c
[12] Savajols H *et al* 1999 *Nucl. Phys.* A **654** 1027c
[13] Gadea A *et al* 2004 *Eur. Phys. J.* A **20** 193
[14] Shepherd S L *et al* 1999 *Nucl. Instrum. Methods Phys. Res.* A **434** 373
[15] Vigezzi E and Winther A 1989 *Ann. Phys. (NY)* **192** 432
[16] Winther A 1994 *Nucl. Phys.* A **572** 191
[17] Winther A 1995 *Nucl. Phys.* A **594** 203
[18] Winther A program GRAZING, htpp:/www.to.infn.it/~nanni/grazing (unpublished)
[19] Corradi L and Pollarolo G 2006 *Nucl. Phys. News* **15** N.4
[20] 2006 *Fusion06: Int. Conf. on Reaction Mechanisms and Nuclear Structure at the Coulomb Barrier (Venezia, Italy, 19–23 Mar.) (AIP Conf. Proc.* vol 853*)* ed L Corradi *et al* (New York: Melville)
[21] 2008 *Fusion08: Int. Conf. on New Aspects of Heavy Ion Collisions Near the Coulomb Barrier (Chicago, USA, 22–26 Sept.) (AIP Conf. Proc.* vol 1098*)* ed K E Rehm *et al* (New York: Melville)
[22] Levon A I *et al* 2009 *Phys. Rev.* C **79** 014318
[23] Sugiyama Y, Tomita Y, Yamanouti Y, Hamada S, Ikuta T, Fujita H and Napoli D R 1997 *Phys. Rev.* C **55** R5
[24] Rehm K E, Beck C, van den Berg A, Kovar D G, Lee L L, Ma W C, Videbaek F and Wang T F 1990 *Phys. Rev.* C **42** 2497
[25] Sapotta K, Bass R, Hartmann W, Noll H, Renfordt R E and Stelzer K 1985 *Phys. Rev.* C **31** 1297
[26] Corradi L *et al* 1996 *Phys. Rev.* C **54** 201
[27] Montagnoli G, Scarlassara F, Beghini S, Dal Bello A, Segato G F, Stefanini A M, Ackermann D, Corradi L, Lin C J and He J H 2000 *Nucl. Instrum. Methods Phys. Res.* A **454** 306
[28] Cormier T 1987 *Annu. Rev. Nucl. Part. Sci.* **37** 537
[29] Betts R R *et al* 1987 *Phys. Rev. Lett.* **59** 978
[30] Speer J, von Oertzen W, Schüll D, Wilpert M, Bohlen H G, Gebauer B, Kohlmeyer B and Puhlofer F 1991 *Phys. Lett.* B **259** 422
[31] Jiang C L, Rehm K E, Gehring J, Glagola B, Kutschera W, Rhein M and Wuosmaa A H 1994 *Phys. Lett.* B **337** 59
[32] Szilner S *et al* 2005 *Phys. Rev.* C **71** 044610
[33] Corradi L *et al* 1990 *Nucl. Instrum. Methods Phys. Res.* A **287** 461
[34] Schüll D 1983 *Proc. Hans Geiger Symp. Detectors in Heavy Ion Reactions (Berlin, 1982) (Lecture Notes in Physics* vol 178*)* (Berlin: Springer) p 80
[35] von Oertzen W *et al* 1987 *Z. Phys.* A **326** 463
[36] Kunkel R *et al* 1990 *Z. Phys.* A **336** 71
[37] Cunsolo A *et al* 2002 *Nucl. Instrum. Methods* A **481** 48
[38] Montagnoli G *et al* 2005 *Nucl. Instrum. Methods Phys. Res.* A **547** 455
[39] Beghini S *et al* 2005 *Nucl. Instrum. Methods Phys. Res.* A **551** 364
[40] Pullanhiotan S, Rejmund M, Navin A, Mittig W and Bhattacharyya S 2008 *Nucl. Instrum. Methods Phys. Res.* A **593** 343
[41] Szilner S *et al* 2007 *Phys. Rev.* C **76** 024604
[42] Juutinen S *et al* 1987 *Phys. Lett.* B **192** 307
[43] Cocks J F C *et al* 1997 *Phys. Rev. Lett.* **78** 2920
[44] Wu C Y *et al* 1995 *Phys. Rev.* C **51** 173
[45] Simon M W *et al* 2000 *Nucl. Instrum. Methods Phys. Res.* A **452** 205
[46] Peter I *et al* 2003 *Eur. Phys. J.* A **16** 509
[47] Corradi L *et al* 2000 *Phys. Rev.* C **61** 024609
[48] Alder K and Winther A 1975 *Electromagnetic Excitation* (Amsterdam: North-Holland)
[49] Broglia R, Pollarolo G and Winther A 1981 *Nucl. Phys.* A **361** 379
[50] Pollarolo G, Broglia R and Winther A 1983 *Nucl. Phys.* A **406** 369
[51] Quesada J M, Pollarolo G, Broglia R A and Winther A 1985 *Nucl. Phys.* A **442** 381
[52] Corradi L, Stefanini A M, Lin C J, Beghini S, Montagnoli G, Scarlassara F, Pollarolo G and Winther A 1999 *Phys. Rev.* C **59** 261

[53] Corradi L *et al* 2002 *Phys. Rev.* C **66** 024606
[54] Buttle P J A and Goldfarb L J B 1966 *Nucl. Phys.* **78** 409
[55] Brink D M 1972 *Phys. Lett.* B **40** 37
[56] Sørensen J H, Pollarolo G and Winther A 1989 *Phys. Lett.* B **225** 41
[57] Ö Akyüz and Winther A 1981 Nuclear structure and heavy-ion physics *Proc. Int. School of Physics 'Enrico Fermi', Course LXXVII, Varenna* ed R A Broglia and R A Ricci (Amsterdam: North-Holland)
[58] Corradi L, Stefanini A M, Ackermann D, Beghini S, Montagnoli G, Petrache C, Scarlassara F, Dasso C H, Pollarolo G and Winther A 1994 *Phys. Rev.* C **49** R2875
[59] Jiang C L, Rehm K E, Esbensen H, Blumenthal D J, Crowell B, Gehring J, Glagola B, Schiffer J P and Wuosmaa A H 1998 *Phys. Rev.* C **57** 2393
[60] Esbensen H, Jiang C L and Rehm K E 1998 *Phys. Rev.* C **57** 2401
[61] Esbensen H and Landowne S 1989 *Nucl. Phys.* A **492** 473
[62] Dasso C H and Pollarolo G 1985 *Phys. Lett.* B **155** 223
[63] Pollarolo G 2008 *Phys. Rev. Lett.* **100** 252701
[64] Esbensen H 1981 *Nucl. Phys.* A **352** 147
[65] Rowley N, Satchler G R and Stelson P H 1991 *Phys. Lett.* B **254** 25
[66] Timmers H, Leigh J R, Dasgupta M, Hinde D J, Lemmon R C, Mein J C, Morton C R, Newton J O and Rowley N 1995 *Nucl. Phys.* A **584** 190
[67] Mitsuoka S, Ikezoe H, Nishio K, Tsuruta K, Jeong S C and Watanabe Y 2007 *Phys. Rev. Lett.* **99** 182701
[68] Pollarolo G and Winther A 2000 *Phys. Rev.* C **62** 054611
[69] Bayman B F and Chen J 1982 *Phys. Rev.* C **26** 1509
[70] Maglione E, Pollarolo G, Vitturi A, Broglia R A and Winther A 1985 *Phys. Lett.* B **162** 59
[71] von Oertzen W and Vitturi A 2001 *Rep. Prog. Phys.* **64** 1247
[72] von Oertzen W *et al* 2004 *Eur. Phys. J.* A **20** 153
[73] Corradi L *et al* 2001 *Phys. Rev.* C **63** 021601
[74] Gavron A 1980 *Phys. Rev.* C **21** 230
[75] Szilner S *et al* 2004 *Eur. Phys. J.* A **21** 87
[76] Caurier E, Martínez-Pinedo G, Nowacki F, Poves A and Zuker A P 2005 *Rev. Mod. Phys.* **77** 427
[77] Rejmund M *et al* 2000 *Eur. Phys. J.* A **8** 161
[78] Kadi M *et al* 2000 *Phys. Rev.* C **61** 034307
[79] Pantelica D *et al* 2005 *Phys. Rev.* C **72** 024304
[80] Bucurescu D *et al* 2005 *Phys. Rev.* C **71** 034315